

Zonostrophic instabilities in magnetohydrodynamic Kolmogorov flow

Azza M. Algaatheem*, Andrew D. Gilbert and Andrew S. Hillier

Department of Mathematics and Statistics, University of Exeter, Exeter EX4 4QF, UK

(March 10, 2023)

This paper concerns the classic problem of stability of the Kolmogorov flow $\mathbf{u} = (0, \sin x)$ in the infinite (x, y) -plane. A mean magnetic field of strength B_0 is introduced and the MHD linear stability problem is studied for modes with a wave-number k in the y -direction, and sometimes a Bloch wavenumber ℓ in the x -direction. The key parameters governing the problem are the Reynolds number ν^{-1} , magnetic Prandtl number P , and dimensionless magnetic field strength B_0 corresponding to an inverse magnetic Mach number. The mean magnetic field can also be taken to have an arbitrary direction in the (x, y) -plane and a mean x -directed flow U_0 can be incorporated, in the most general formulation.

First the paper considers Kolmogorov flow with a y -directed mean magnetic field, which for convenience we refer to as ‘vertical’. Taking $\ell = 0$, the suppression of the classic hydrodynamic instability is observed with increasing field strength B_0 . A branch of strong-field instabilities occurs when the magnetic Prandtl number P is less than unity, as found recently by A.E. Fraser, I.G. Cresser and P. Garaud (*J. Fluid Mech.* **949**, A43, 2022). Analytical results based on eigenvalue perturbation theory in the limit $k \rightarrow 0$ support the numerics for both weak-field and strong-field instabilities, and show their origin in the coupling of large-scale weakly damped modes with x -wavenumber $n = 0$, to smaller-scale modes having $n = \pm 1$.

The paper then considers the case of ‘horizontal’ or x -directed mean magnetic field. Here the unperturbed state consists of steady, wavy magnetic field lines distorted by the underlying Kolmogorov flow, and with the driving body force balancing both viscosity and the Lorentz force. As the magnetic field is increased from zero, the purely hydrodynamic instability is suppressed again, but for stronger fields a new branch of instabilities appears. Allowing a non-zero Bloch wavenumber ℓ allows further instability, and in some circumstances when the system is hydrodynamically stable, arbitrarily weak magnetic fields can give growing modes, via the instability taking place on large scales in x and y . Numerical results are presented together with eigenvalue perturbation theory in the limits $k, \ell \rightarrow 0$. The theory gives analytical approximations for growth rates and thresholds that are in good agreement with those computed.

1. Introduction

The Kolmogorov flow, a periodic flow forced at a single wavenumber, is a classic flow to study due to its simplicity and its wide applications to the study of different geophysical and astrophysical systems. Its stability to linear disturbances is a classic problem first posed by Kolmogorov and studied by Meshalkin and Sinai (1961). These authors made use of continued fraction expansions to establish properties of the growth rate $p(k)$, where k is a wavenumber in the y -direction, and determined a critical Reynolds number of $\text{Re}_c = \sqrt{2}$. Close to onset of

*Corresponding author. Email: aa965@exeter.ac.uk

instability, for Re slightly larger than $\sqrt{2}$, it is large scale modes in y that are destabilised; more precisely, for $Re = \sqrt{2}(1 + 3k^2 + \dots)$ the most unstable mode has wave number $k \ll 1$. This property allows the development of amplitude equations governing the flow on large space and time scales, obtained by Nepomniashchii (1976) and Sivashinsky (1985). Numerical simulations by She (1987) showed evolution from the most unstable scale to larger scales via an inverse cascade of vortex pairings, for a large scale allowed only in the y -direction. For large scales in both x - and y -directions, Sivashinsky (1985) showed evolution to a large-scale flow with chaotic temporal fluctuations, further explored in Lucas and Kerswell (2014, 2015).

The stability problem posed by Kolmogorov is such a fundamental building block in stability theory that it has been elaborated in several studies by incorporating further physical phenomena. Frisch *et al.* (1996) included a β -effect, giving the gradient of a background planetary vorticity distribution; the gradient is oriented along the x direction (again following our conventions rather than those of the original paper), so that it does not interact directly with the transverse, basic state Kolmogorov flow \mathbf{u}_0 . These authors derived an amplitude equation near to onset for a large scale in y , which they called the β -Cahn-Hilliard equation. For $\beta = 0$ this reduces to the PDE of Sivashinsky (1985) and simulations show that the inverse cascade of structures to large scales in y is arrested by the β -effect. These authors characterise the fundamental instability of the Kolmogorov flow as due to a negative eddy viscosity, in other words that the large-scale y -dependent modes have growth rate $p = -\nu_E k^2 + \dots$ where the eddy viscosity ν_E changes sign from positive below the threshold $Re_c = \sqrt{2}$, to negative above, so destabilising the flow on large scales with the fastest growing modes determined by the next terms in this series (Dubrulle and Frisch 1991).

In terms of the geophysical motivation for these stability problems, any orientation of the background vorticity gradient, parameterised by β , with respect to the Kolmogorov flow is of interest. Manfroi and Young (2002) allow an arbitrary angle α between flow and gradient in a study of linear stability and nonlinear evolution using amplitude equations generalising those of Sivashinsky (1985) and Frisch *et al.* (1996). They find that the linear problem shows a delicate dependence of critical Reynolds number on angle α when unstable modes are allowed to adopt arbitrarily large scales in x and y . Another effect of geophysical relevance that may be included is stratification. Balmforth and Young (2002) considered the sinusoidal flow in the (x, z) plane with gravity in the $-z$ direction and the flow directed in x , sinusoidal in z . These authors determined the behaviour of linear instabilities, depending on Reynolds, Richardson and Prandtl numbers, and derived an amplitude equation generalising that of Sivashinsky (1985). Simulations show that the inverse cascade of She (1987) is arrested by the presence of stratification over a wide range of parameters.

Relevant to the present paper, in astrophysical applications it is natural to introduce a magnetic field and study the coupled MHD system; as general motivation we note, for example, that the interaction between magnetic field, shear, and convection remains poorly understood in the solar tachocline (Hughes *et al.* 2007). Boffetta *et al.* (2000) considered the case in which a sinusoidal magnetic field (maintained by a source term in the induction equation) sits in a motionless fluid. This magnetic Kolmogorov system shows instabilities and an amplitude equation gives an inverse cascade to large scales. The recent paper Fraser *et al.* (2022) considers a background uniform magnetic field $\mathbf{B}_0 = (0, B_0)$ that is aligned with the Kolmogorov flow; this has no effect on the basic state flow but the elasticity of field lines affects perturbations depending on y , through the Lorentz force. These authors observe magnetic suppression of the instability first discussed by Meshalkin and Sinai (1961), as one might intuitively expect, but also two new families of unstable modes which only exist in the presence of magnetic

field. One family exists for magnetic Prandtl number $P < 1$, for arbitrarily strong magnetic fields, provided the Reynolds number is above a threshold depending on P . This is studied numerically and growth rates obtained through asymptotic approximations for $k \ll 1$; these authors refer to these modes as Alfvén–Dubrulle–Frisch modes, as the instability can be linked to a change of sign of the eddy viscosity (Dubrulle and Frisch 1991).

Study of Kolmogorov flow instabilities is relevant to the formation of zonal flows in forced fluid systems, so-called ‘zonostrophic instability’ (Galperin *et al.* 2006). This process of jet formation has now been observed in many simulations, observations and experiments; see the representative studies, Vallis and Maltrud (1993), Read *et al.* (2007), Farrell and Ioannou (2008), Scott and Dritschel (2012), Srinivasan and Young (2012), Bouchet *et al.* (2013), and Parker and Krommes (2014). Related to our work, Tobias *et al.* (2007) incorporated a magnetic field aligned with the x -direction of a planar fluid system with a β -effect present, a vorticity gradient in y . The system was driven by a body force with a given characteristic spatial scale. These authors observed the formation of jets in the x -direction for zero magnetic field, but then the suppression of jets, even at quite weak field strengths B_0 . For fixed non-dimensional β , forcing and viscosity $\nu = 10^{-4}$, this process was explored by means of a series of runs with varying magnetic field strength B_0 and magnetic diffusivity η , and evidence for a threshold scaling law of $B_0^2 \sim \eta$ was observed (Tobias *et al.* 2011). Constantinou and Parker (2018) analysed Kelvin–Orr shearing wave dynamics for Rossby/Alfvén waves and the interplay between Reynolds and Maxwell stresses, providing evidence for this $B_0^2 \sim \eta$ threshold for jet formation. Durston and Gilbert (2016) focused on the couplings between large-scale zonal flow and zonal field in the presence of waves, calculating an effective viscosity and effective magnetic diffusivity, plus an effective cross transport term in which current gradients can drive the zonal vorticity; this and other transport effects are discussed in Chechkin (1999), Kim (2007), and Leprovost and Kim (2009). Parker and Constantinou (2019) interpret the presence or otherwise of jets in terms of the competition between a positive magnetic eddy viscosity term and a negative, purely hydrodynamic eddy viscosity. Note that while these studies of zonostrophic instability have many qualitative features in common with the topic of Kolmogorov flow instability, there are key differences that make any direct comparison difficult, even of scaling laws. The reason is that the studies referred to in this paragraph use a forcing which has a given spatial scale but is random in time, and the forcing is kept fixed while other parameters such as the viscosity, magnetic diffusivity, magnetic field or β are varied. In non-dimensional terms, the input parameter is a Grashof number (formed from forcing strength, length scale and viscosity) in these systems (Durston and Gilbert 2016); the Reynolds number is then a diagnostic parameter, and can vary considerably in different regimes depending on the dominant balances in the Navier–Stokes equation between the forcing term, inertial term, viscous term and Lorentz force. However for stability of Kolmogorov flow, the basic state is fixed while the forcing is adjusted to maintain this: the input parameter is a Reynolds number, instead.

In the present paper we return to the classic set-up of steady, planar, Kolmogorov flow $\mathbf{u}_0 = (0, \sin x)$ and consider the effect on its stability from magnetic field in the x - and y -directions. We find it convenient to refer to magnetic field in the y -direction, parallel to the flow as ‘vertical field’ and magnetic field in the x -direction, aligned with possible jet formation, as ‘horizontal field’ (even though gravity/stratification are not involved in our study). In §2 we set up the equations solved for linear perturbations with vertical magnetic field and in section 3 present numerical and analytical results, showing growth rates, thresholds and unstable mode structure. This section has common elements with the recent paper Fraser *et al.* (2022) (published while the present paper was in preparation); however we find it useful to set out the numerical results to compare with the later horizontal field case, and we present new

analytical results in §3.1 for the ‘weak vertical field branch’. The ‘strong vertical field branch’ in §3.2 is a primary focus for Fraser *et al.* (2022), and we give an alternative, matrix-based derivation of the asymptotic growth rate they obtain. Section 4 sets up the equations for horizontal magnetic field, with numerical results supported by analytical approximations in the limit $k \rightarrow 0$ given in §5, together with the case of non-zero Bloch wavenumber ℓ , and §6 offers concluding discussion. Further analytical and numerical results will appear in Algaatheem (2023). To keep the main body of the paper compact, we have developed analytical theory in appendices, building up in order of complexity rather than in the order in which the results are used. The method employed is perturbation theory for eigenvalues and eigenvectors of a matrix; naturally this is equivalent to methods used by other authors, but we find that is a systematic way of handling problems of increasing complexity, and gives insight into how couplings between individual flow and field modes can drive an instability.

2. Governing equations: vertical field

Our starting point is the system of equations for incompressible, constant density MHD, written in the form

$$\partial_t \mathbf{u} + \mathbf{u} \cdot \nabla \mathbf{u} = -\nabla p + \mathbf{j} \times \mathbf{b} + \nu \nabla^2 \mathbf{u} + \mathbf{f}, \quad (2.1)$$

$$\partial_t \mathbf{b} + \mathbf{u} \cdot \nabla \mathbf{b} = \mathbf{b} \cdot \nabla \mathbf{u} + \eta \nabla^2 \mathbf{b}, \quad (2.2)$$

$$\nabla \cdot \mathbf{u} = 0, \quad \nabla \cdot \mathbf{b} = 0, \quad \mathbf{j} = \nabla \times \mathbf{b}. \quad (2.3)$$

Here the magnetic field is represented in velocity units, and \mathbf{f} is an externally imposed rotational body force, used to maintain a given basic state for the system. In dimensional units this basic state is the Kolmogorov flow, namely the unidirectional flow in the (x, y) -plane specified by

$$\mathbf{u}_0 = \mathcal{U}(0, \sin(x/\mathcal{L})). \quad (2.4)$$

We use the length \mathcal{L} and velocity \mathcal{U} as the basis of our non-dimensionalisation, which results in the same equations (2.1–2.3) above but having ν now identified as an inverse Reynolds number, with $\text{Re} = \nu^{-1}$, and η as an inverse magnetic Reynolds number, with $\text{Rm} = \eta^{-1}$. The non-dimensional Kolmogorov flow is then

$$\mathbf{u}_0 = (0, \sin x). \quad (2.5)$$

Note that we drop the z -components of vectors where we can. A key quantity we will need is the magnetic Prandtl number

$$P = \text{Rm}/\text{Re} = \nu/\eta. \quad (2.6)$$

We will consider flows \mathbf{u} and magnetic fields \mathbf{b} lying in the (x, y) -plane, independent of z . For this we use a stream function ψ and vector potential a defined by

$$\mathbf{u} = (\psi_y, -\psi_x), \quad \mathbf{b} = (a_y, -a_x). \quad (2.7)$$

The governing equations may then be written in terms of the evolution of a scalar vorticity

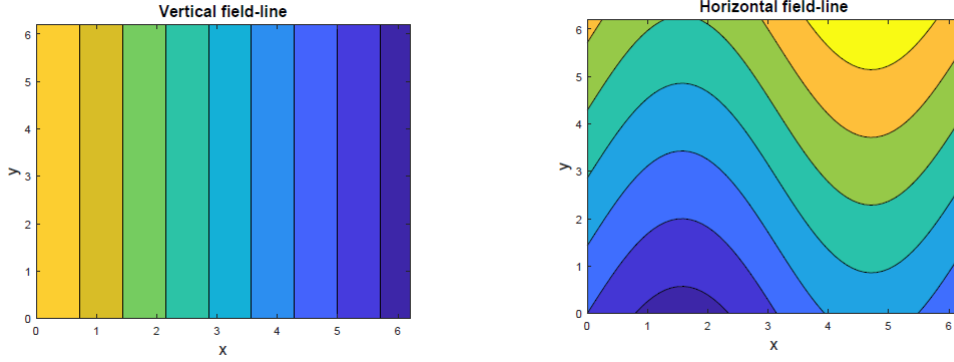


Figure 1. The magnetic field basic state for (a) vertical field (in §§2, 3), (b) horizontal field (in §§4, 5), with $B_0 = 0.7$, $\eta = 0.5$. In each case fields lines are depicted as contours of the corresponding vector potential a_0 , with $\mathbf{b}_0 = (\partial_y a_0, -\partial_x a_0)$.

ω , and a :

$$\partial_t \omega + \mathcal{J}(\omega, \psi) = \mathcal{J}(j, a) + \nu \nabla^2 \omega + g, \quad (2.8)$$

$$\partial_t a + \mathcal{J}(a, \psi) = \eta \nabla^2 a, \quad (2.9)$$

$$\omega = -\nabla^2 \psi, \quad j = -\nabla^2 a. \quad (2.10)$$

Here \mathcal{J} is the Jacobian of two functions in the plane and g is the z -component of the curl of the body force \mathbf{f} .

We begin with the study of the stability of Kolmogorov flow in the presence of vertical magnetic field (that is, y -directed field) of strength B_0 (Fraser *et al.* 2022). Aiming for the most general set-up we also include a uniform horizontal flow (that is, an x -directed flow) of strength U_0 . We therefore adopt the following steady solution of the equations as our basic state,

$$\mathbf{u}_0 = (U_0, \sin x), \quad \mathbf{b}_0 = (0, B_0), \quad \mathbf{f} = (0, \nu \sin x + U_0 \cos x), \quad (2.11)$$

or in our scalar-based formulation

$$\psi_0 = U_0 y + \cos x, \quad \omega_0 = \cos x, \quad a_0 = -B_0 x, \quad j_0 = 0, \quad g = \nu \cos x - U_0 \sin x. \quad (2.12)$$

The basic state magnetic field is shown in figure 1(a). The stability problem is parameterised by the four quantities $\{\nu, B_0, P, U_0\}$. Note that while the mean horizontal flow specified by the parameter U_0 could be removed by a Galilean transformation, the Kolmogorov flow would then become a travelling wave. Thus, given we always take a steady Kolmogorov flow in the form (2.5), the effect of U_0 cannot be eliminated by this means.

To study the stability of this basic state we linearise, replacing

$$\psi = \psi_0 + \psi_1 + \dots, \quad \omega = \omega_0 + \omega_1 + \dots, \quad a = a_0 + a_1 + \dots, \quad j = j_0 + j_1 + \dots, \quad (2.13)$$

and, dropping the subscript 1, we deduce the linear system

$$\partial_t \omega + U_0 \omega_x + \sin x (\omega_y - \psi_y) = B_0 j_y + \nu \nabla^2 \omega, \quad (2.14)$$

$$\partial_t a + U_0 a_x + \sin x a_y = B_0 \psi_y + \eta \nabla^2 a, \quad (2.15)$$

$$\omega = -\nabla^2 \psi, \quad j = -\nabla^2 a. \quad (2.16)$$

We now expand the fields in Fourier modes in x as

$$(\psi, \omega, a, j) = e^{pt+ilx+iky} \sum_n (F_n, G_n, H_n, J_n) e^{inx} + \text{c.c.} \quad (2.17)$$

Here p is the complex growth rate of the mode, k is the wavenumber in the y -direction with $k > 0$ without loss of generality, and ℓ is a Bloch or Floquet wavenumber in the x -direction satisfying $-1/2 < \ell \leq 1/2$.

Substituting these series into the linear equations (2.14–2.16) results in an infinite system of equations. For $\ell = 0$ these may be written in the form:

$$pG_n = -[\nu(n^2 + k^2) + inU_0]G_n + \frac{k}{2} \left(\frac{1}{(n-1)^2 + k^2} - 1 \right) G_{n-1} \quad (2.18)$$

$$- \frac{k}{2} \left(\frac{1}{(n+1)^2 + k^2} - 1 \right) G_{n+1} + ikB_0(n^2 + k^2)H_n,$$

$$pH_n = -[\eta(n^2 + k^2) + inU_0]H_n - \frac{k}{2} H_{n-1} + \frac{k}{2} H_{n+1} + \frac{ikB_0}{n^2 + k^2} G_n, \quad (2.19)$$

and for $\ell \neq 0$ we simply replace $n \rightarrow n + \ell$ wherever it appears (except as a subscript). This provides an eigenvalue problem giving a discrete set of eigenvalues with a dependence $p(k, \ell, \nu, B_0, P, U_0)$ in general, and the real part of the growth rate is unchanged on the replacement $(k, \ell) \rightarrow (-k, -\ell)$.

For a numerical solution we restrict $-N \leq n \leq N$ for some integer N (typical values are 16, 32) and solve a discrete matrix problem written in the pentadiagonal form

$$p \begin{pmatrix} \vdots \\ G_n \\ H_n \\ \vdots \end{pmatrix} = \begin{pmatrix} \ddots & \ddots & \ddots & & & & \\ \ddots & \otimes & 0 & \otimes & \otimes & \otimes & 0 & \ddots \\ \ddots & 0 & \otimes & \otimes & \otimes & 0 & \otimes & \ddots \\ \ddots & \ddots & \ddots & \ddots & \ddots & \ddots & \ddots & \ddots \end{pmatrix} \begin{pmatrix} \vdots \\ G_n \\ H_n \\ \vdots \end{pmatrix}, \quad (2.20)$$

where \otimes denotes the only non-zero entries. At a specified truncation N the $(4N+2) \times (4N+2)$ matrix is set up in Matlab, and an eigenvalue p with maximum real part is calculated. For a given parameter set $\{\nu, B_0, P, U_0\}$ the maximum real growth rate is defined as

$$\text{Re } p_{\max}(\nu, B_0, P, U_0) = \max_{k, \ell} \text{Re } p(k, \ell, \nu, B_0, P, U_0), \quad (2.21)$$

with the maximum taken over a grid of k and ℓ values.

In what follows we will start by taking $U_0 = 0$, $\ell = 0$ and only vary the vertical wavenumber k . The maximisation is then taken over a finite range of k -values, typically 100 values in the range $0 \leq k \leq 1$, and any complex eigenvalues appear in complex conjugate pairs. We let $k_{\max}(\nu, B_0, P)$ be the corresponding maximising wave number, and we attach the appropriate (zero or positive) imaginary part to give $p_{\max}(\nu, B_0, P)$ as the (maximum) complex instability growth rate. It is then often instructive to plot $\text{Re } p_{\max}$, $\text{Im } p_{\max}$ and k_{\max} .

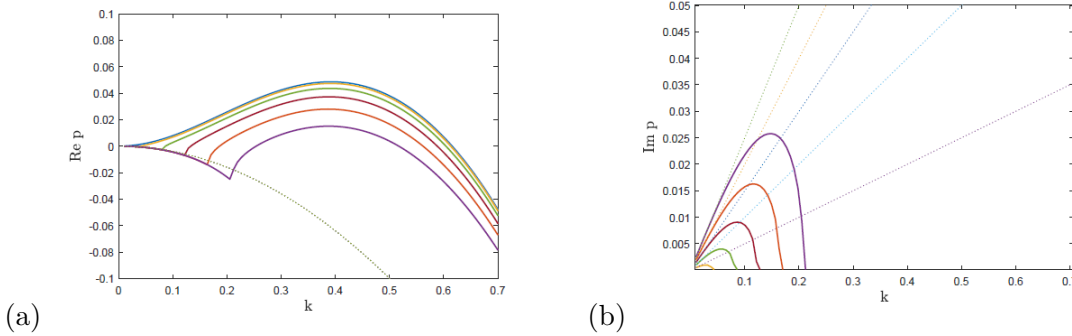


Figure 2. Instability growth rate p for vertical magnetic field as a function of wave number k (with $U_0, \ell = 0$) for $\nu = \eta = 0.4$ ($P = 1$), and $B_0 = 0$ (blue), $B_0 = 0.05$ (orange), $B_0 = 0.10$ (green), $B_0 = 0.15$ (dark red), $B_0 = 0.20$ (red) and $B_0 = 0.25$ (purple). Panels (a) and (b) show $\text{Re } p$ and $\text{Im } p$ respectively, and dotted curves show the Alfvén wave branch in (3.22).

3. Numerical and analytical results: vertical field

We use the numerical code as described above to produce eigenvalues so that we can explore the dependence on parameters. Our starting point is to investigate the effect of increasing the vertical magnetic field strength B_0 on the classic hydrodynamic instability of Kolmogorov flow.

3.1. Weak vertical field branch

Figure 2(a) shows the real part of the growth rate $p(k, \nu, B_0, P)$ for $\nu = \eta = 0.4$ and so $P = 1$, plotted against k for given values of the magnetic field strength B_0 . Here B_0 is increased from zero in steps of 0.05 as we read down the family of curves. The top curve relates to the purely hydrodynamic case. As we increase B_0 we note two effects: first the peak is reduced, in other words the magnetic field acts to suppress the instability, as found by Fraser *et al.* (2022). Secondly, for large scales, namely small k , a new branch of decaying modes appears, with growth rates largely independent of field strength. Figure 2(b) shows the imaginary part of the growth rate p . This is zero for the purely hydrodynamic case and remains zero for this branch as it is suppressed by the field. The new branch for low k has a non-zero imaginary part which becomes more prominent as B_0 is increased and we read up the curves. Some investigation shows that the new branch is in fact a damped Alfvén wave on the vertical magnetic field. For zero background flow \mathbf{u}_0 , a vertical field supports Alfvén waves with

$$p = \pm ik \sqrt{B_0^2 - \frac{1}{4}(\nu - \eta)^2 k^2} - \frac{1}{2}(\nu + \eta)k^2, \quad (3.22)$$

and the real and imaginary parts are shown dotted in figure 2. Since the Alfvén waves are modified by the background Kolmogorov flow, the agreement is not exact, but this is clearly the origin of these small- k damped modes.

A typical unstable mode is shown in figure 3 for parameter values corresponding to the peak in the lowest curve in figure 2(a), that is for the strongest field used. We observe the perturbation streamfunction ψ in panel (a) showing clear zonostrophic jets, and corresponding changes to the magnetic vector potential in panel (b); Fraser *et al.* (2022) refer to these as sinuous Kelvin–Helmholtz modes. As the instabilities we observe here are obtained from the

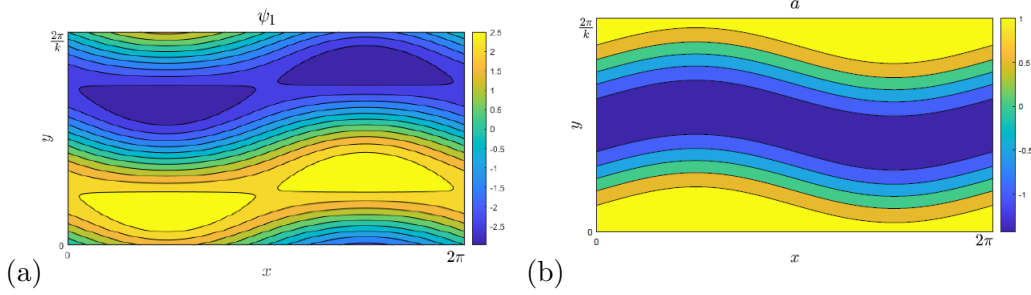


Figure 3. Structure of a typical unstable mode, with $B_0 = 0.25$, $\nu = \eta = 0.4$, $k = 0.4$; (a) shows the stream function ψ and (b) the vector potential a .

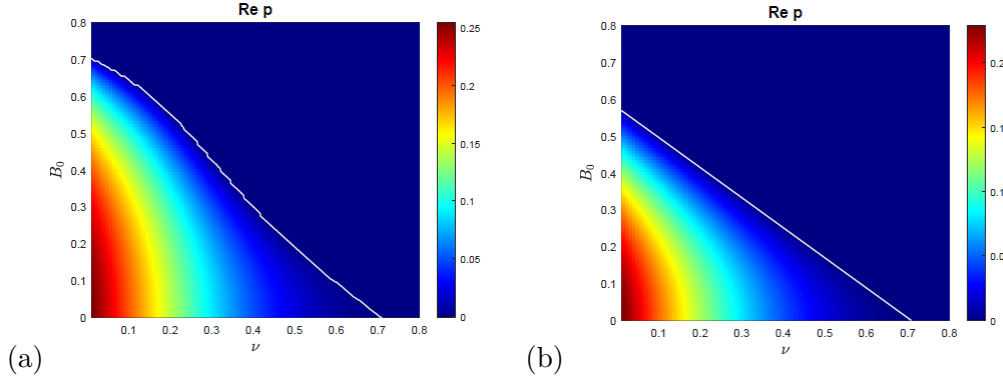


Figure 4. Instability growth rate $\text{Re } p_{\max}$ for vertical field plotted in the (ν, B_0) plane for $P = 1$, $\ell = 0$, $U_0 = 0$. Panel (a) shows the numerical computation of growth rates with the threshold $\text{Re } p_{\max} = 0$ given by a white curve, and panel (b) the analytical maximum growth rate from (3.24) and threshold from (3.25).

hydrodynamic problem as we increase B_0 from small values, we refer to this as the *weak vertical field branch*, to be contrasted with a strong field branch we encounter shortly.

Having seen a particular example of how the magnetic field suppresses the hydrodynamic instability by plotting $p(k, \nu, B_0, P)$, we now show results where we maximise over k for each set of the parameters. Figure 4(a) shows numerical results for $\text{Re } p_{\max}(\nu, B_0, P)$ with $P = 1$ as a colour plot across the (ν, B_0) -plane. The white curve shows the threshold for instability (actually set for $\text{Re } p_{\max}$ having a small positive value). The horizontal axis $B_0 = 0$ is the hydrodynamic case, where the white curve crosses at $\nu_c = 1/\sqrt{2}$. Instability occurs in the region below the white curve, and we can see that it is suppressed as B_0 increases, up to the point where $B_0 \simeq 0.7$ and the instability is entirely eliminated. We do not show $\text{Im } p_{\max}$, which is zero within the region of instability.

We can develop perturbation theory (as in, for example, Frisch *et al.* 1996, Manfroi and Young 2002) to calculate approximate growth rates valid for $k \rightarrow 0$. In appendix C we give the details. One key result is the formula (C.19),

$$p(k, \nu, B_0, P) = -\frac{\sqrt{2}P}{1+P^2} B_0^2 + 2\left(\frac{1}{\sqrt{2}} - \nu\right)k^2 - \frac{3}{\sqrt{2}}k^4 + \dots, \quad (3.23)$$

giving the growth rate, and showing clearly how the effect of the magnetic field is to suppress the hydrodynamic $B_0 = 0$ instability (as seen in figure 2(a)). For unstable modes it is necessary that $\nu < 1/\sqrt{2}$ and in this case maximising the growth rate over values of k gives

$$p_{\max}(\nu, B_0, P) = -\frac{\sqrt{2}P}{1+P^2} B_0^2 + \frac{\sqrt{2}}{3} \left(\frac{1}{\sqrt{2}} - \nu\right)^2, \quad k_{\max}^2 = \frac{\sqrt{2}}{3} \left(\frac{1}{\sqrt{2}} - \nu\right). \quad (3.24)$$

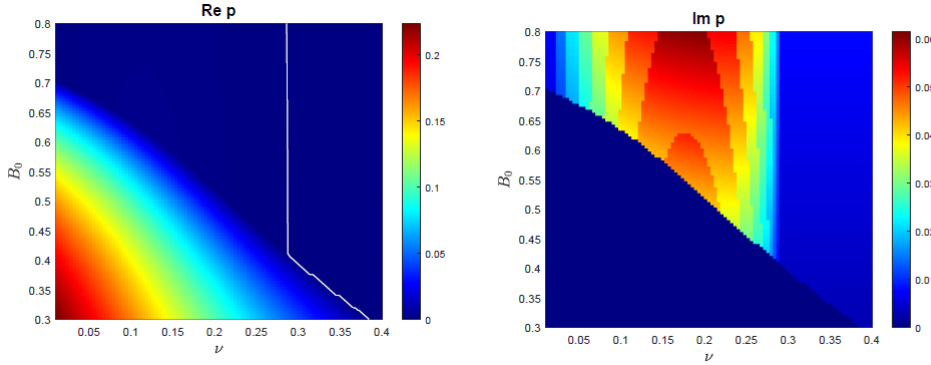


Figure 5. Shown are (a) instability growth rate $\text{Re } p_{\max}$ and (b) frequency $\text{Im } p_{\max}$ for vertical field plotted in the (ν, B_0) plane, with $P = \frac{1}{2}$. The results shown are obtained computationally and the white curve in panel (a) shows zero growth rate.

Putting $p_{\max} = 0$ gives the threshold of instability as the straight line in the (ν, B_0) -plane:

$$B_0(\nu, P) = \sqrt{\frac{1 + P^2}{3P}} \left(\frac{1}{\sqrt{2}} - \nu \right). \quad (3.25)$$

Figure 4(b) shows the theoretical growth rate and the threshold marked by a white (straight) line, showing good agreement with the full numerics. The perturbation theory is developed about the point $\nu_c = 1/\sqrt{2}$, $B_0 = 0$ of the onset of the hydrodynamic instability. Hence the agreement is particularly good near this point; elsewhere the theory gives results that are qualitatively correct only, for example the theoretical value of B_0 which suppresses instability for all ν is given by

$$B_0 \simeq B_* = \sqrt{\frac{1 + P^2}{6P}}, \quad (3.26)$$

with $B_* \simeq 0.58$ for $P = 1$ in panel (b), which is a little lower than the actual value $B_* \simeq 0.7$ seen for the numerical results in panel (a).

3.2. Strong vertical field branch

Although the magnetic field acts to suppress the instability for magnetic Prandtl number $P = 1$, this is not the whole picture, and investigations for $P < 1$ show the presence of a *strong vertical field branch*, as found by Fraser *et al.* (2022). Figure 5 shows (a) the real part and (b) imaginary part of the growth $p_{\max}(\nu, B_0, P)$ for $P = 1/2$, that is $\eta = 2\nu$. The threshold $\text{Re } p_{\max} = 0$ is shown as a white curve in both figures. Looking from the bottom of the panel 5(a) (increasing B_0) we see that the curving white line, showing the weak field branch in panel 4(a), turns to become a near-vertical line, demarcating a new branch with non-zero frequency $\text{Im } p_{\max}$ evident in panel 5(b).

This strong vertical field branch is analysed in appendix B, using a scaling in which $B_0 = O(k^{-1})$ as $k \rightarrow 0$. The perturbation theory then involves a leading order undamped Alfvén wave with frequency $p_0 = ikB_0 = O(1)$. The coupling of this wave with the flow field leads to potential instability with a growth rate given in (B.9) as:

$$\text{Re } p = \frac{\frac{1}{4}\nu\eta(\eta - \nu)k^2}{\nu^2\eta^2 + k^2B_0^2(\nu + \eta)^2} - \frac{1}{2}(\nu + \eta)k^2 + \dots. \quad (3.27)$$

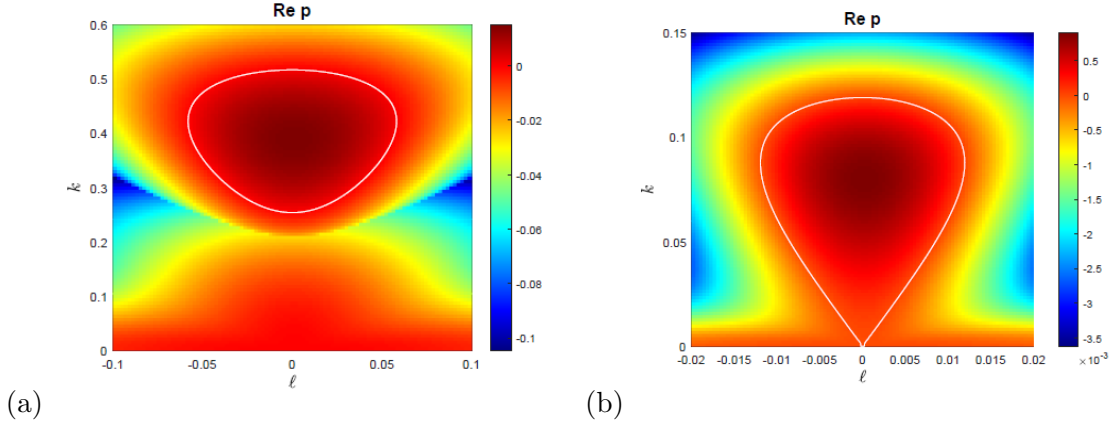


Figure 6. Instability growth rate p for vertical field as a function of (ℓ, k) for (a) $\nu = \eta = 0.4$ ($P = 1$) with $B_0 = 0.25$, and (b) $\nu = 0.2$, $\eta = 0.4$ ($P = 0.5$) with $B_0 = 0.7$.

An equivalent expression is found in Fraser *et al.* (2022) by approximating a quartic dispersion relation. Evidently we need $\eta > \nu$ for instability, in other words $P < 1$; the instability of the large-scale Alfvén wave appears to take a double-diffusive form. As discussed in the appendix, the stability threshold (B.9) of Fraser *et al.* (2022) is also obtained from this equation as

$$\nu < \nu_* = \sqrt{\frac{P}{2} \frac{1-P}{1+P}}. \quad (3.28)$$

For example if $P = 1/2$ then $\nu_* = 1/\sqrt{12} \simeq 0.28$, in good agreement with the vertical white lines in figure 5. Thus the instability persists for arbitrarily large magnetic fields, provided the viscosity is below this Prandtl-number dependent threshold, in other words provided the Reynolds number $\text{Re} = \nu^{-1} > \nu_*^{-1}$.

All the above results have been taken for Bloch wave number $\ell = 0$. Introducing ℓ brings in an extra degree of freedom and allows the possibility of new instabilities. However in the vertical field case increasing $|\ell|$ from zero has only a stabilising effect (Fraser *et al.* 2022). For example figure 6 shows growth rates in the (ℓ, k) -plane for weak and strong field cases in panels (a) and (b). The vertical axis gives $\ell = 0$ and we see an island of unstable modes in each case. However to either side of the vertical axis, the growth rates are diminished and allowing $\ell \neq 0$ has little impact. For this reason we will not consider ℓ further for the vertical field case, except to mention that the theory in appendix B may be extended to incorporate $\ell \neq 0$, as detailed in Algaatheem (2023).

4. Governing equations: horizontal field, with $U_0 = 0$

In this section we study the stability of Kolmogorov flow in the presence of horizontal field B_0 , and to reduce the complexity of the problem we restrict to the case of zero horizontal mean flow $U_0 = 0$. We thus adopt the following basic state, a steady solution of the equations (2.1–2.3):

$$\mathbf{u}_0 = (0, \sin x), \quad \mathbf{b}_0 = (B_0, \eta^{-1} B_0 \cos x), \quad \mathbf{f} = (0, (\nu + \eta^{-1} B_0^2) \sin x), \quad (4.29)$$

or in the scalar formulation

$$\psi_0 = \cos x, \quad \omega_0 = \cos x, \quad a_0 = B_0 y - \eta^{-1} B_0 \sin x, \quad j_0 = -\eta^{-1} B_0 \sin x, \quad g = (\nu + \eta^{-1} B_0^2) \cos x. \quad (4.30)$$

The basic state magnetic field is shown in figure 1(b), with horizontal field lines distorted by the background Kolmogorov flow, becoming increasingly extended in the limit of small η . Note, to pick up a comment in the introduction, that the body force required to maintain the Kolmogorov flow increases with field strength B_0 and with magnetic Reynolds number $\text{Rm} = \eta^{-1}$, unlike in many large-scale simulations of zonostrophic instability, where the magnitude of a random forcing is held fixed, while other parameters are varied.

The stability problem is parameterised by $\{\nu, B_0, P, U_0 = 0\}$. The corresponding linear system is

$$\partial_t \omega + \sin x (\omega_y - \psi_y) = B_0 j_x + \eta^{-1} B_0 \cos x (j_y - a_y) + \nu \nabla^2 \omega, \quad (4.31)$$

$$\partial_t a + \sin x a_y = B_0 \psi_x + \eta^{-1} B_0 \cos x \psi_y + \eta \nabla^2 a, \quad (4.32)$$

$$\omega = -\nabla^2 \psi, \quad j = -\nabla^2 a, \quad (4.33)$$

where the fields represent the perturbation to the basic state. The resulting equations for the Fourier modes in x are

$$\begin{aligned} pG_n = & -\nu(n^2 + k^2)G_n + \frac{k}{2} \left(\frac{1}{(n-1)^2 + k^2} - 1 \right) G_{n-1} - \frac{k}{2} \left(\frac{1}{(n+1)^2 + k^2} - 1 \right) G_{n+1} \\ & + inB_0(n^2 + k^2)H_n + \frac{ikB_0}{2\eta} [(n-1)^2 + k^2 - 1] H_{n-1} + \frac{ikB_0}{2\eta} [(n+1)^2 + k^2 - 1] H_{n+1}, \end{aligned} \quad (4.34)$$

$$\begin{aligned} pH_n = & -\eta(n^2 + k^2)H_n - \frac{k}{2} H_{n-1} + \frac{k}{2} H_{n+1} \\ & + \frac{inB_0}{n^2 + k^2} G_n + \frac{ikB_0}{2\eta} \frac{1}{(n-1)^2 + k^2} G_{n-1} + \frac{ikB_0}{2\eta} \frac{1}{(n+1)^2 + k^2} G_{n+1}, \end{aligned} \quad (4.35)$$

for $\ell = 0$ and, as elsewhere, for $\ell \neq 0$ we replace n by $n + \ell$. This infinite system of linear equations may then be truncated and set up as a matrix eigenvalue problem, analogously to that in (2.20) for vertical field; the matrix now takes a heptadiagonal form.

5. Numerical and analytical results: horizontal field

We have used Matlab to obtain growth rates $p(k, \ell, \nu, B_0, P)$ (here $U_0 = 0$) and we focus first on the case $\ell = 0$.

5.1. Instability for Bloch wave number $\ell = 0$

With zero Bloch wave number ℓ , the instability has periodicity 2π in the x -direction and $2\pi/k$ in the y -direction. Figure 7 shows plots of the growth rate $p(k, \nu, B_0, P)$ against k for $\nu = \eta = 0.1$ ($P = 1$) and B_0 increasing as detailed in the caption. Focusing on the real part of p in panel (a) we observe that the magnetic field initially suppresses the instability, going from

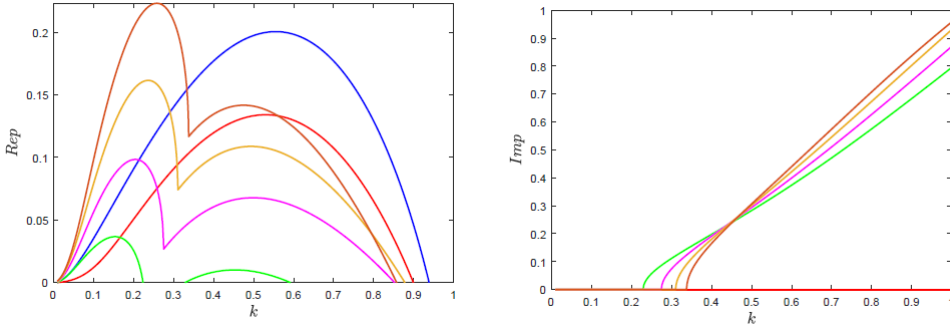


Figure 7. Instability growth rate p for horizontal field as a function of k (and $\ell = 0$) for $\nu = \eta = 0.1$ ($P = 1$), with $B_0 = 0$ (blue), 0.05 (red), 0.1 (green), 0.15 (purple), 0.20 (orange) and 0.25 (dark orange). Panels (a) and (b) show $\text{Re } p$ and $\text{Im } p$ respectively.

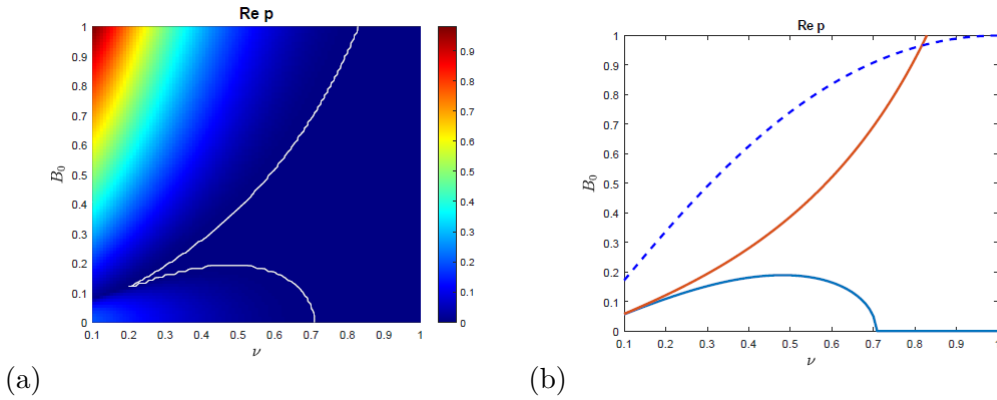


Figure 8. Instability growth rate $\text{Re } p$ for horizontal field plotted in the (ν, B_0) plane for $P = 1$, $\ell = 0$, $U_0 = 0$. Panel (a) shows the numerical computation of growth rates with the threshold given by a white curve, and panel (b) the analytical thresholds from (5.37) for the flow branch (blue), and from (5.41) for the field branch (dark orange). In panel (b) the dashed line is the threshold (5.47) for $\ell \neq 0$ instabilities discussed later.

the blue $B_0 = 0$ curve to the lower, red $B_0 = 0.05$ curve. However increasing B_0 further, the green $B_0 = 0.1$ curve reveals a double-peaked growth rate and then these two peaks increase as B_0 is increased, as indicated in the figure caption. For these stronger fields, the second peak is the lower of the two, and is associated with non-zero imaginary part $\text{Im } p$ of the growth rate, as shown in panel (b), while the dominant instability of the first peak has $\text{Im } p = 0$. In fact for all our studies of instability for horizontal field with $U_0 = 0$ and $\ell = 0$, we observe that the dominant instability is always direct or non-oscillatory, that is $\text{Im } p = 0$.

To give a more global picture of these results for horizontal field, we now show $p_{\max}(\nu, B_0, P)$ as a colour plot in the (ν, B_0) -plane with $P = 1$ in figure 8(a), with the white line denoting the instability threshold $\text{Re } p = 0$. For modest magnetic fields we observe the suppression of the purely hydrodynamic instability as in the case of vertical field in figure 4. However as B_0 is increased another branch of instability emerges from the bottom left of the panel 8(a) and shows increasing growth rates, particularly for smaller viscosities ν . This new branch of instabilities is perhaps not surprising (Durstun and Gilbert 2016), given that the basic state horizontal field in (4.29) and depicted in figure 1(b) has a wavy structure, and for $P = 1$ becomes increasingly convoluted as $\eta = \nu$ is decreased. Other values of P give plots that are similar in structure.

To gain analytical results and understanding, in appendix A we discuss perturbation theory for the horizontal field system, taking the limit $k \rightarrow 0$ while retaining B_0 and other parameters

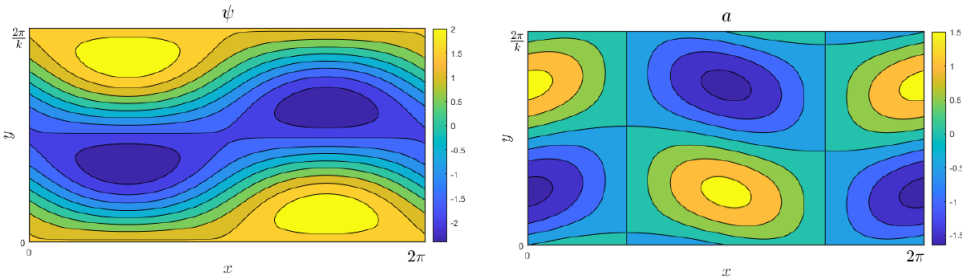


Figure 9. A typical unstable mode, with $B_0 = 0.05$, $\nu = \eta = 0.1$, $k = 0.5$, from the flow or G_0 branch; (a) shows the stream function ψ and (b) the vector potential a .

of order unity. The resulting leading order equations involving G_0 , $G_{\pm 1}$, H_0 and $H_{\pm 1}$ split into the two independent 3×3 matrix systems giving the two branches of instability evident in figure 8(a). We discuss them in turn.

The first system involves G_0 and not H_0 , in other words is dominated by a large-scale flow and not a large-scale field. We call this the G_0 or *flow branch* of the horizontal field instability. Analysis gives equation (A.31), which we reproduce here as

$$p = \left[\frac{1}{2\nu} \frac{\nu^2 - B_0^2 P^2 (2 + P)}{\nu^2 + B_0^2 P} - \nu \right] k^2 + \dots \quad (5.36)$$

This gives the leading growth rate as a function of the parameters times k^2 ; it represents an eddy viscosity ν_E seen by large-scale modes and the instability is marked by this quantity becoming negative. While it is not possible to maximise this expression over k to gain a complete analysis of the instability, it does give the instability threshold $\text{Re } p = 0$, by setting $[\dots] = 0$ to obtain

$$B_0^2 = \frac{\nu}{P} \frac{1 - 2\nu^2}{2\nu + 2P + P^2}. \quad (5.37)$$

This formula is plotted as the blue curve in panel 8(b) and shows good agreement with the numerical results for the lower branch in panel 8(a). For $B_0 = 0$ we recover the hydrodynamic result $\nu_c = 1/\sqrt{2}$, and this analysis tells us how this hydrodynamic instability, dominated by the large-scale flow in G_0 , is suppressed by interaction with the magnetic field. If we maximise B_0^2 as a function of ν in (5.37), we find that this occurs at

$$2\nu^2 = -Q + \sqrt{Q^2 + Q}, \quad Q = 2P + P^2, \quad (5.38)$$

and putting this into B_0^2 gives an unwieldy expression for the threshold value B_* above which the horizontal field suppresses the Kolmogorov instability. We do not present it here but give further discussion in §6.

Note also that from (5.37),

$$B_0 \simeq \frac{\nu}{P\sqrt{2+P}}, \quad \nu \rightarrow 0, \quad (5.39)$$

and so the instability emerges with this slope from the origin $\nu = 0$, $B_0 = 0$ of the figure. A typical example of the instability is shown in figure 9: the stream function in panel (a) shows its nature as a zonal instability giving horizontal jets, with modifications to the field in panel (b).

The second system arising from perturbation theory involves H_0 and not G_0 : it is dominated by a large-scale magnetic field and so we refer to this as the H_0 or *field branch* of the

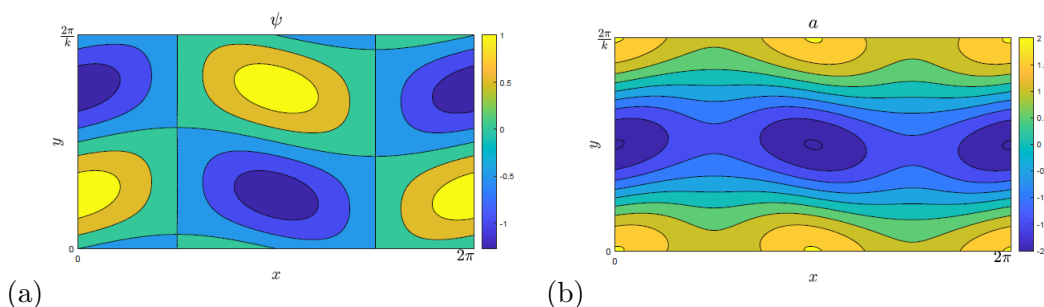


Figure 10. A typical unstable mode, with $B_0 = 0.25$, $\nu = \eta = 0.1$, $k = 0.25$. from the field or H_0 branch; (a) shows the stream function ψ and (b) the vector potential a .

horizontal field instability. The result of perturbation theory gives (A.37), reproduced here as

$$p = \left[\frac{P}{2\nu} \frac{-\nu^2 + 3B_0^2 P}{\nu^2 + B_0^2 P} - \frac{\nu}{P} \right] k^2 + \dots \quad (5.40)$$

The onset of instability again can be interpreted as a transport quantity becoming negative, here the eddy magnetic diffusivity η_E (see Chechkin 1999). Note that this instability, being a directly growing instability does not connect to the strong-field branch of the vertical field (which is an over-stable wave).

The threshold for instability is given by $[\dots] = 0$ or

$$B_0^2 = \frac{\nu^2}{P} \frac{P^2 + 2\nu^2}{3P^2 - 2\nu^2}. \quad (5.41)$$

This curve is plotted on figure 8(b) in red and again shows good agreement with the numerical results for the field branch in panel (a). Note that for fixed P , $B_0 \rightarrow \infty$ as $\nu \rightarrow \nu_*$ with

$$\nu_* = P\sqrt{3/2}, \quad (5.42)$$

and so a viscosity larger than this is enough to prevent the field branch instability no matter how strong the field. We also have for small fields and viscosities that the threshold (5.41) is given by

$$B_0 \simeq \frac{\nu}{\sqrt{3P}}, \quad \nu \rightarrow 0, \quad (5.43)$$

and so for $P = 1$ both thresholds (5.39) and (5.43) emerge from the origin with the same slope, though for general P they are different. A typical example of the instability is given in figure 10. The perturbation flow now does not have a zonostrophic jet structure, but shows closed eddies in panel (a). Panel (b) however shows a banded structure in the magnetic field (showing the dominant role of H_0), and indicates a tendency for the background mean field to segregate into bands of stronger and weaker horizontal field.

5.2. Instability for Bloch wave number $\ell \neq 0$

Finally, we consider horizontal field for the case of non-zero ℓ . This allows an instability to take up a scale $2\pi/k$ in the y -direction and $2\pi/\ell$, as $\ell \rightarrow 0$, in the x -direction. It turns out that instabilities can occur for $\ell \neq 0$ even when the system is stable for $\ell = 0$, in the case of horizontal field (unlike the situation for vertical field).

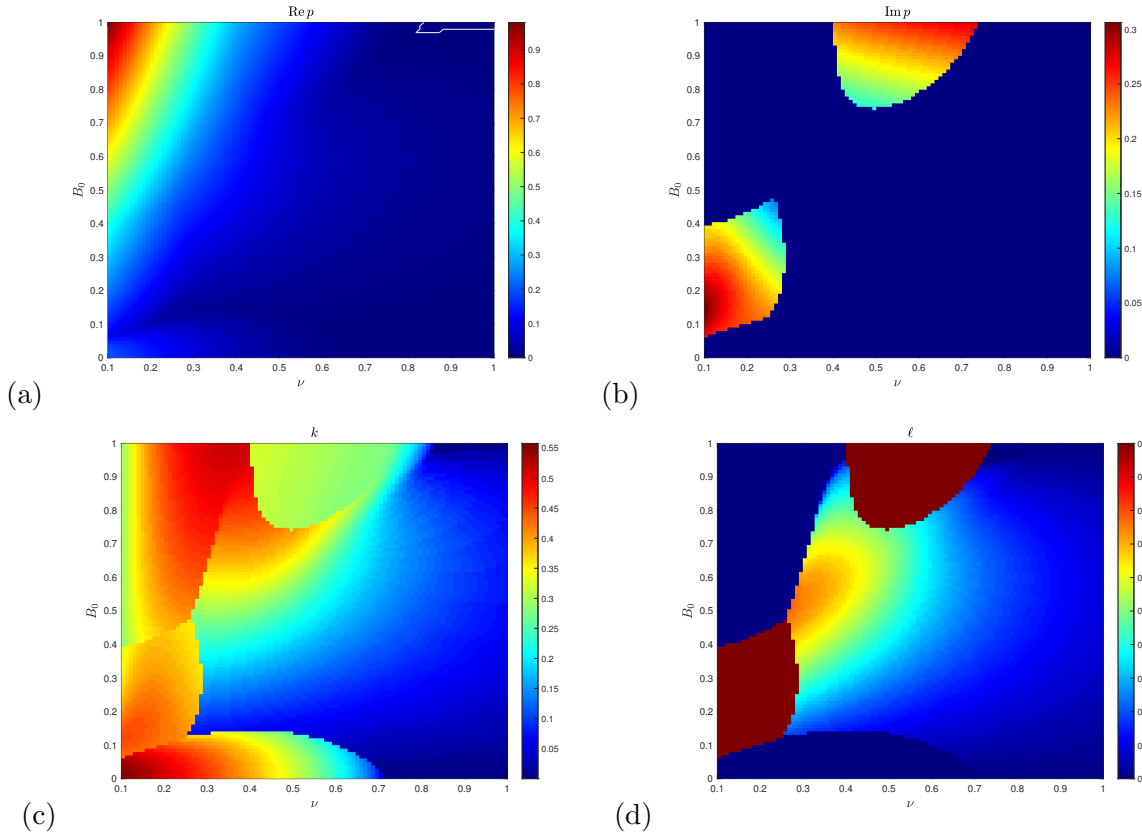


Figure 11. (a) Instability growth rate $\text{Re } p$ and (b) imaginary part $\text{Im } p$ shown for horizontal field, plotted in the (ν, B_0) with $P = 1$, $U_0 = 0$, and $\ell \neq 0$. The maximising values of k and of ℓ are shown in panels (c, d) respectively.

Figure 11(a) shows a similar general structure to figure 8(a), though note that the white curve has all but disappeared. The purely hydrodynamic instabilities are suppressed by increasing B_0 , i.e. the G_0 or flow branch; this is not really visible now in panel (a) but the branch is evident in panel (c) showing k_{\max} , with $\ell_{\max} = 0$ in panel (d) here. Then, the H_0 or field branch of instability appears clearly in panel (a) for larger B_0 . However looking at panels (b) and (d) now the field branch has regions with non-zero imaginary part to the growth rate, regions with ℓ increasing from zero, and regions with ℓ constant at $\ell = 0.5$ indicating instabilities with 4π periodicity in x (further investigated in Algaatheem 2023). Returning to figure 11(a), the reason for the loss of the white curve, compared with figure 8(a), is that there is now a new instability, reliant on having $\ell \neq 0$ which means that almost all of the region of stability in the $\ell = 0$ figure 8(a) is now unstable in figure 11(a). The corresponding growth rates are quite small, and so this is otherwise not immediately evident on these plots.

We therefore turn to theory for $\ell \neq 0$, developed in appendix D, which gives a growth rate in (D.13) of

$$p = \pm B_0 \ell \left[\frac{k^2}{\ell^2 + k^2} \frac{P[\nu^2(P+2) - P^2 B_0^2]}{\nu^2(\nu^2 + P B_0^2)} - 1 \right]^{1/2} + \dots \quad (5.44)$$

This approximation reveals an instability that crucially relies on having a non-zero Bloch wavenumber, $\ell \neq 0$, with ℓ and k both small. If we fix the parameters ν , P and B_0 we can consider the growth rate p as a function in the (ℓ, k) plane. Setting the quantity inside the square root to zero to find a threshold, we see that the region of instability is demarcated by

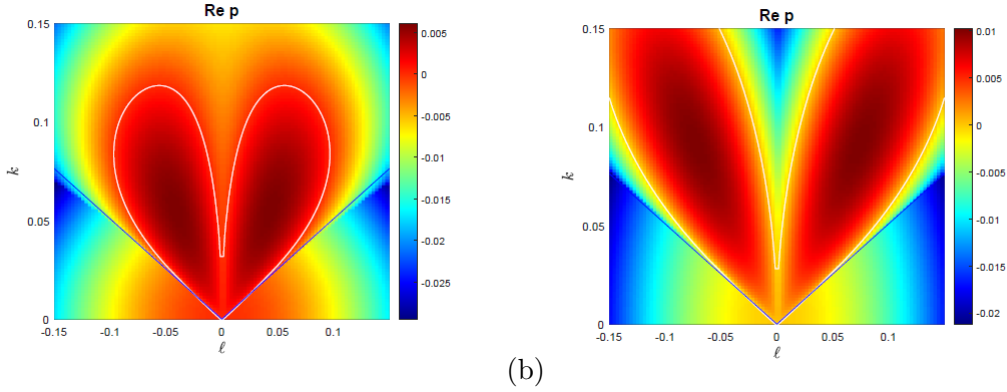


Figure 12. Instability growth rate p for horizontal field as a function of (ℓ, k) for $\nu = \eta = 0.75$ ($P = 1$) with $B_0 = 0.2$, (a) numerical growth rates and (b) approximate growth rates calculated from (5.46).

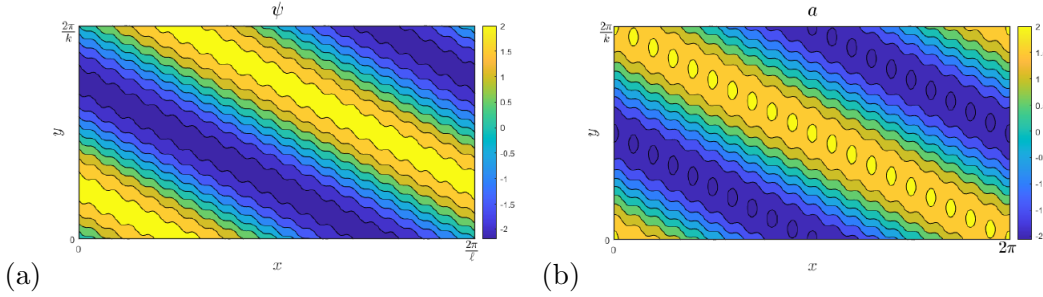


Figure 13. A typical unstable mode, with $\ell = 0.05$, $k = 0.05$, $\nu = \eta = 0.75$, $B_0 = 0.2$; (a) shows the stream function ψ and (b) the vector potential a .

the pair of straight lines given by

$$\frac{k^2}{\ell^2} = \frac{\nu^2(\nu^2 + PB_0^2)}{\nu^2(P^2 + 2P - \nu^2) - PB_0^2(\nu^2 + P^2)}. \quad (5.45)$$

The growth rate p tells us about the instability growth rate as we increase k and ℓ from zero, but to find how this eventually decreases, we would need to go to next order in perturbation theory, which is impractical and unlikely to be informative. To give a qualitative feel for the growth rate we will add on the diffusive suppression term $-\frac{1}{2}(\nu + \eta)k^2$ that is certainly present at next order, and look at

$$p = \pm B_0 \ell \left[\frac{k^2}{\ell^2 + k^2} \frac{P[\nu^2(P + 2) - P^2 B_0^2]}{\nu^2(\nu^2 + PB_0^2)} - 1 \right]^{1/2} - \frac{1}{2} \nu (1 + P^{-1})(k^2 + \ell^2) + O(k^2, \ell^2). \quad (5.46)$$

To see how this works, figure 12(a) shows growth rates plotted in the (ℓ, k) -plane for $B_0 = 0.2$ and $\nu = \eta = 0.75$, parameters corresponding to stability for $\ell = 0$. There is now a region of instability taking a ‘butterfly’ form, outlined by the white curve $\text{Re } p = 0$. The straight blue lines are given by (5.45) and are tangential to the white lines at the origin, confirming the theory. In panel (b) we show an analogous figure for the ‘fixed up’ growth rate in (5.46). The agreement between the results in the two panels (a) and (b) is excellent near the origin, but then further out the agreement is only qualitative, and quite rough, as we might expect. For an example of an unstable configuration, figure 13 shows the flow and field for the fastest growing mode in figure 12. We observe the structure of a large-scale jet-like structure but at an oblique angle to the y -direction, this being allowed by the non-zero Bloch wavenumber ℓ .

Returning to the bigger picture, for instability at a general points in the (ν, B_0) plane we

need the quantity $[\dots]$ inside the square root in (5.44) to be positive for some values of k and ℓ . Equivalently, it corresponds to requiring that the straight lines in (5.45) have a finite slope. It can be checked that this gives a threshold for instability:

$$B_0^2 = \frac{\nu^2(P^2 + 2P - \nu^2)}{P(\nu^2 + P^2)}. \quad (5.47)$$

Values of field smaller than this give instability and so this formula gives the threshold curve in the (ν, B_0) plane for this family of $\ell \neq 0$ instabilities. This threshold is shown as a dashed curve in figure 8(b). We thus see in this panel that allowing $\ell \neq 0$ means that almost the whole of the parameter ranges shown give instability, all except for a small curved triangular region at the top right, and this is in agreement with the white curve obtained numerically in figure 11(a). The agreement is not perfect because the growth rates in the top right corner become small and the unstable region shrinks away in the (ℓ, k) -plane, as the thresholds are approached, and so the precise location of the white curve becomes hard to resolve without further work.

Note that for $P = 1$, from (5.47) the instability is cut off at $\nu = \sqrt{3}$, and in general the instability requires

$$\nu < \nu_* = \sqrt{P(2 + P)}. \quad (5.48)$$

Numerical experimentation shows that for ν less than this value, the region of instability in the (ℓ, k) -plane becomes vanishingly small as B_0 tends to zero or tends to the value given in (5.47). The maximum magnetic field for the $\ell \neq 0$ instability found here is given by maximising B_0 over ν : the maximum occurs at

$$\nu^2 = -P^2 + \sqrt{2P^3(1 + P)}, \quad (5.49)$$

and we pick this up in the final discussion section, §6.

6. Discussion

In this study we have explored instability of the classic Kolmogorov flow in the presence of magnetic field which is either vertical, aligned with the flow, or horizontal, aligned with possible jet formation. In the vertical field case we have obtained new analytical results for the maximum growth rate (3.24) and magnetic field threshold (3.25), that show the suppression of the original instability found by Meshalkin and Sinai (1961) by vertical magnetic field. In particular we have obtained a value B_* in (3.26) as an estimate of the field magnitude required to suppress the Kolmogorov instability. This corresponds to a threshold that is

$$B_*^2 \sim P^{-1} = \frac{\eta}{\nu} \quad (P \ll 1), \quad B_*^2 \sim P = \frac{\nu}{\eta} \quad (P \gg 1). \quad (6.50)$$

For the strong field branch we have confirmed the numerical results of Fraser *et al.* (2022) and provided an alternative derivation of their growth rate formula (3.27) and threshold (3.28). We note that these authors also find a third branch of instabilities, which they term ‘varicose Kelvin–Helmholtz’ modes, which we have not observed at the Reynolds numbers we have used.

The case of horizontal field, broadly relevant to several studies of jet formation where the field is aligned with potential jets (Tobias *et al.* 2007, Durston and Gilbert 2016, Constantinou

and Parker 2018), shows more complex structure, unsurprisingly given the wavy nature of the magnetic field in the basic state, seen in figure 1(b). We observe again the suppression of the purely hydrodynamic instability, the flow or G_0 branch, when the magnetic field strength is increased, with a threshold of $B_0 = B_*$ for complete suppression with B_* given by substituting ν^2 from (5.38) into (5.37). For large P , we have $\nu^2 \simeq 1/4$ while for small P , $\nu^2 \simeq \sqrt{P/2}$. The value of B_* for suppression then amounts to:

$$B_*^2 \sim P^{-1} = \frac{\eta}{\nu} \quad (P \ll 1), \quad B_*^2 \sim P^{-3} = \frac{\eta^3}{\nu^3} \quad (P \gg 1). \quad (6.51)$$

Interestingly this bears comparison with Tobias *et al.* (2007) who have $\nu = 10^{-4}$ fixed and $10^{-1} \leq \eta \leq 10^{-6}$ in their runs. For the greater values of η used, $P \ll 1$ and so a threshold $B_*^2 \sim \eta$ is indicated above, and found in these full numerical simulations. Also, note that at this threshold we have that the forcing magnitude is fixed in magnitude in (4.29) and so there is, at least roughly, a correspondence of working with fixed forcing amplitude as in their paper and the fixed Kolmogorov flow in ours. However we should remark that these authors use a non-zero value of β and we have ℓ zero, and so further work would need to be done to make a sound comparison.

A feature of the horizontal field problem is that for increasing magnetic field strengths a further branch of instabilities emerges, the field or H_0 branch, also seen in Durston and Gilbert (2016). Analytical formulae for the threshold of instability are given for each branch. The field branch exists provided the Reynolds number is above a threshold, $\text{Re} > \nu_*^{-1}$ with ν_* given in (5.42). Allowing a Bloch wavenumber $\ell \neq 0$ in the x -direction, in addition to the wavenumber k in the y -direction, allows a new branch of instabilities. In particular a magnetic field, no matter how weak, can destabilise the Kolmogorov flow provided the Reynolds number $\text{Re} = \nu^{-1} > \nu_*^{-1}$ with ν_* given in (5.48). For example at $P = 1$, the purely hydrodynamic instability is present for $\text{Re} > \sqrt{2}$ but an MHD instability is present for arbitrarily weak but non-zero horizontal magnetic field provided $\text{Re} > 1/\sqrt{3}$. For sufficiently large magnetic field this instability is again suppressed, and making use of (5.49) (with $\nu^2 \simeq \sqrt{2P^3}$ for small P and $\nu \simeq (\sqrt{2} - 1)P^2$ for large P) we find a threshold

$$B_*^2 \sim 1 \quad (P \ll 1), \quad B_*^2 \sim P = \frac{\nu}{\eta} \quad (P \gg 1). \quad (6.52)$$

Note that the order of limits could be important: in our discussion in this paper we are fixing any value of P and then allowing k and ℓ to tend to zero. Other limits are possible and could be explored by appropriate scalings in our calculations.

Underlying our study is matrix eigenvalue perturbation theory as set out in the appendices, a flexible tool for these types of problems. We find it gives greater clarity than using a multiple scales formulation or applying perturbation theory to roots of a polynomial, even though all these methods are ultimately equivalent. Note that while many of the instabilities seen by us and by other authors can be characterised as involving a negative eddy viscosity term $-\nu_E k^2$ or a negative eddy magnetic diffusivity term $-\eta_E k^2$ at large scales, the growth rate $p(k, \ell)$ in the case of horizontal field shows a complicated dependence on k and ℓ in (5.44). Although this $\ell \neq 0$ instability occurs at arbitrarily large scales, it cannot be categorised as involving a simple negative eddy transport effect. This arises because we are applying perturbation theory to a repeated eigenvalue of the limiting $k \rightarrow 0$, $\ell \rightarrow 0$ problem. Looking to the future, it would be interesting to pursue further research on the Kolmogorov flow as an MHD system, particularly on the nonlinear evolution of instabilities and inverse cascades (Fraser *et al.* 2022, Algahtem 2023), and on the interaction of magnetic field with a β -effect and Rossby waves.

Appendix A: Horizontal field, with $U_0 = 0$, $\ell = 0$

First, let us outline the general principles of our approximate analysis of growth rates in this and other appendices. We have in each case an infinite system of coupled linear equations, for example (4.34, 4.35) in the case of horizontal field with $U_0 = 0$ and $\ell = 0$. In the limit $k \rightarrow 0$ of large-scale modes, we can reduce the calculation of the growth rate to eigenvalues of a finite matrix. The key point to note is that the $n = 0$ modes G_0 and H_0 are distinguished from all other modes by being weakly damped, as $p_{\text{visc}} = -\nu k^2$ or $p_{\text{diff}} = -\eta k^2$ by molecular diffusion with $k \ll 1$. On the other hand other modes with $|n| > 0$ are relatively strongly damped, with $p_{\text{visc}} = -\nu(n^2 + k^2)$ or $p_{\text{diff}} = -\eta(n^2 + k^2)$. So we need to keep the $n = 0$ modes as these are most easily destabilised in the system. How are they destabilised? This is through the coupling from $n = 0$ to low $n \neq 0$ modes and then back to $n = 0$, and via these couplings the unstable mode can draw energy from the basic state Kolmogorov flow $\mathbf{u}_0 = (0, \sin x)$. It then follows that we typically expect to see effects only at second order or beyond in terms of perturbation theory, and this then will involve G_n and H_n for $n = -1, 0, 1$ only. Thus we can truncate the system and then use perturbation theory for the eigenvalues of a finite matrix, with $k \ll 1$ as an expansion parameter.

Thus we set to work on the horizontal system of equations (4.34, 4.35) in Fourier space. These are truncated to just the modes $G_0, G_{\pm 1}, H_0$ and $H_{\pm 1}$, with

$$pG_0 = -\nu k^2 G_0 - \frac{k}{2} \frac{k^2}{1+k^2} G_{-1} + \frac{k}{2} \frac{k^2}{1+k^2} G_1 + \frac{ikB_0}{2\eta} k^2 H_{-1} + \frac{ikB_0}{2\eta} k^2 H_1, \quad (\text{A.1})$$

$$pH_0 = -\eta k^2 H_0 - \frac{k}{2} H_{-1} + \frac{k}{2} H_1 + \frac{ikB_0}{2\eta} \frac{1}{1+k^2} G_{-1} + \frac{ikB_0}{2\eta} \frac{1}{1+k^2} G_1, \quad (\text{A.2})$$

$$pG_{\pm 1} = -\nu(1+k^2)G_{\pm 1} \pm \frac{k}{2} \frac{1-k^2}{k^2} G_0 \pm iB_0(1+k^2)H_{\pm 1} + \frac{ikB_0}{2\eta}(-1+k^2)H_0, \quad (\text{A.3})$$

$$pH_{\pm 1} = -\eta(1+k^2)H_{\pm 1} \mp \frac{k}{2} H_0 \pm iB_0 \frac{1}{1+k^2} G_{\pm 1} + \frac{ikB_0}{2\eta} \frac{1}{k^2} G_0. \quad (\text{A.4})$$

We now express these equations in terms of G_0, H_0 and the fields

$$G_{\pm} = \frac{1}{2}(G_1 \pm G_{-1}), \quad H_{\pm} = \frac{1}{2}(H_1 \pm H_{-1}); \quad (\text{A.5})$$

we rescale $G_0 = G'_0 k^2$ and for convenience we set $\tilde{B}_0 = B_0/\eta$. The resulting equations then break up into two uncoupled systems. The first involves only G'_0 on the large scale,

$$pG'_0 = -\nu k^2 G'_0 + k(1+k^2)^{-1} G_- + ik\tilde{B}_0 H_+, \quad (\text{A.6})$$

$$pG_- = -\nu(1+k^2)G_- + \frac{1}{2}k(1-k^2)G'_0 + iB_0(1+k^2)H_+, \quad (\text{A.7})$$

$$pH_+ = -\eta(1+k^2)H_+ + iB_0(1+k^2)^{-1}G_- + \frac{1}{2}ik\tilde{B}_0 G'_0, \quad (\text{A.8})$$

while the second involves only H_0 on the large scale,

$$pH_0 = -\eta k^2 H_0 + kH_- + ik\tilde{B}_0(1+k^2)^{-1}G_+, \quad (\text{A.9})$$

$$pH_- = -\eta(1+k^2)H_- - \frac{1}{2}kH_0 + iB_0(1+k^2)^{-1}G_+, \quad (\text{A.10})$$

$$pG_+ = -\nu(1+k^2)G_+ + iB_0(1+k^2)H_- + \frac{1}{2}ik\tilde{B}_0(-1+k^2)H_0, \quad (\text{A.11})$$

We deal with these two branches in turn, using eigenvalue perturbation theory.

A.1. Outline of approach

Having reduced the problem to the calculation of eigenvalues p for two systems of equations for $k \ll 1$, one for (A.6–A.8) and one for (A.9–A.10), we outline the method that is common to all the approximations in the paper. In each case we write the governing eigenvalue problem in a matrix form (see (A.24, A.32) below) where the matrix M depends on k , \mathbf{v} is the eigenvector and p the eigenvalue:

$$M\mathbf{v} = p\mathbf{v}. \quad (\text{A.12})$$

We may rescale some quantities in the matrix M (using a prime to denote these) and we then proceed to expand M in powers of k as

$$M = M_0 + kM_1 + k^2M_2 + \dots, \quad (\text{A.13})$$

and likewise \mathbf{v} and p . For the limit $k \rightarrow 0$ we solve

$$(M_0 + kM_1 + \dots)(\mathbf{v}_0 + k\mathbf{v}_1 + \dots) = (p_0 + kp_1 + \dots)(\mathbf{v}_0 + k\mathbf{v}_1 + \dots), \quad (\text{A.14})$$

order by order in k . Here we set out the first few orders in a convenient form:

$$p_0\mathbf{v}_0 = M_0\mathbf{v}_0, \quad (\text{A.15})$$

$$p_1\mathbf{v}_0 = (M_0 - p_0)\mathbf{v}_1 + M_1\mathbf{v}_0, \quad (\text{A.16})$$

$$p_2\mathbf{v}_0 = (M_0 - p_0)\mathbf{v}_2 + M_2\mathbf{v}_0 + M_1\mathbf{v}_1 - p_1\mathbf{v}_1, \quad (\text{A.17})$$

$$p_3\mathbf{v}_0 = (M_0 - p_0)\mathbf{v}_3 + M_3\mathbf{v}_0 + M_2\mathbf{v}_1 + M_1\mathbf{v}_2 - p_2\mathbf{v}_1 - p_1\mathbf{v}_2, \quad (\text{A.18})$$

$$p_4\mathbf{v}_0 = (M_0 - p_0)\mathbf{v}_4 + M_4\mathbf{v}_0 + M_3\mathbf{v}_1 + M_2\mathbf{v}_2 + M_1\mathbf{v}_3 - p_3\mathbf{v}_1 - p_2\mathbf{v}_2 - p_1\mathbf{v}_3. \quad (\text{A.19})$$

First we choose an eigenvalue p_0 and corresponding eigenvector \mathbf{v}_0 of M_0 ; at the level of M_0 the mode is undamped and so the real part of p_0 is zero. Assuming this is a simple (non-repeated eigenvalue) there is also a single left eigenvector \mathbf{w}_0 with $\mathbf{w}_0(M_0 - p_0) = 0$. With (A.15) thus dealt with, we note that we gain successive eigenvalues from applying \mathbf{w}_0 to the left of the remaining equations, so that

$$p_1\mathbf{w}_0\mathbf{v}_0 = \mathbf{w}_0M_1\mathbf{v}_0, \quad (\text{A.20})$$

$$p_2\mathbf{w}_0\mathbf{v}_0 = \mathbf{w}_0(M_2\mathbf{v}_0 + M_1\mathbf{v}_1 - p_1\mathbf{v}_1), \quad (\text{A.21})$$

$$p_3\mathbf{w}_0\mathbf{v}_0 = \mathbf{w}_0(M_3\mathbf{v}_0 + M_2\mathbf{v}_1 + M_1\mathbf{v}_2 - p_2\mathbf{v}_1 - p_1\mathbf{v}_2), \quad (\text{A.22})$$

$$p_4\mathbf{w}_0\mathbf{v}_0 = \mathbf{w}_0(M_4\mathbf{v}_0 + M_3\mathbf{v}_1 + M_2\mathbf{v}_2 + M_1\mathbf{v}_3 - p_3\mathbf{v}_1 - p_2\mathbf{v}_2 - p_1\mathbf{v}_3). \quad (\text{A.23})$$

In this way once having chosen the eigenvalue p_0 to perturb from (A.15) together with \mathbf{v}_0 and \mathbf{w}_0 , we find p_1 from (A.20). We then need \mathbf{v}_1 from (A.16) and while $M_0 - p_0$ is not invertible, having fixed the value of p_1 , there is a solution for \mathbf{v}_1 . It is not unique, but this does not matter as we shall see. We can then calculate p_2 from (A.21) and so forth. We will go up to the level of p_4 in some of our calculations below.

A.2. Flow or G_0 branch

Having set out our general approach we return to the first system (A.6–A.8), which involves a dominant large-scale flow in G_0 and no large-scale field, with

$$M = \begin{pmatrix} -\nu k^2 & k(1+k^2)^{-1} & ik\tilde{B}_0 \\ \frac{1}{2}k(1-k^2) & -\nu(1+k^2) & iB_0(1+k^2) \\ \frac{1}{2}ik\tilde{B}_0 & iB_0(1+k^2)^{-1} & -\eta(1+k^2) \end{pmatrix}, \quad \mathbf{v} = \begin{pmatrix} G'_0 \\ G_- \\ H_+ \end{pmatrix}. \quad (\text{A.24})$$

For this branch we expand M to give:

$$M_0 = \begin{pmatrix} 0 & 0 & 0 \\ 0 & -\nu & iB_0 \\ 0 & iB_0 & -\eta \end{pmatrix}, \quad M_1 = \begin{pmatrix} 0 & 1 & i\tilde{B}_0 \\ \frac{1}{2} & 0 & 0 \\ \frac{1}{2}i\tilde{B}_0 & 0 & 0 \end{pmatrix}, \quad M_2 = \begin{pmatrix} -\nu & 0 & 0 \\ 0 & -\nu & iB_0 \\ 0 & -iB_0 & -\eta \end{pmatrix}. \quad (\text{A.25})$$

Note that the inverse of the non-trivial 2×2 block of M_0 is

$$\begin{pmatrix} -\nu & iB_0 \\ iB_0 & -\eta \end{pmatrix}^{-1} = \Delta \begin{pmatrix} -\eta & -iB_0 \\ -iB_0 & -\nu \end{pmatrix}, \quad \Delta^{-1} = \nu\eta + B_0^2, \quad (\text{A.26})$$

where Δ is the inverse of the appropriate determinant.

We are ready to solve order by order in k . At leading order (A.15) we choose

$$p_0 = 0, \quad \mathbf{v}_0 = (1, 0, 0)^T, \quad \mathbf{w}_0 = (1, 0, 0). \quad (\text{A.27})$$

At next order, we use (A.20) and have

$$M_1 \mathbf{v}_0 = (0, \frac{1}{2}, \frac{1}{2}i\tilde{B}_0)^T, \quad p_1 = 0. \quad (\text{A.28})$$

Given this we now solve (A.16) for \mathbf{v}_1 , to obtain

$$\mathbf{v}_1 = \frac{1}{2}\Delta(0, \eta - \tilde{B}_0 B_0, iB_0 + i\nu\tilde{B}_0)^T. \quad (\text{A.29})$$

Here we have used the inverse (A.26) of the 2×2 block of M_0 to find a solution for \mathbf{v}_1 . We could add on an arbitrary multiple of \mathbf{v}_0 to this, but this would only change the (irrelevant) normalisation of the eigenvector \mathbf{v} in our calculation — any solution is acceptable.

Finally at $O(k^2)$ we find from (A.21) the value of p_2 and, recalling that $\tilde{B}_0 = B_0/\eta$, this gives

$$p = p_2 k^2 + \dots = \left[\frac{1}{2}\Delta(\eta - 2B_0^2/\eta - B_0^2\nu/\eta^2) - \nu \right] k^2 + \dots, \quad (\text{A.30})$$

which is, with the Prandtl number $P = \nu/\eta$,

$$p = \left(\frac{1}{2\nu} \frac{\nu^2 - B_0^2 P^2 (2 + P)}{\nu^2 + B_0^2 P} - \nu \right) k^2 + \dots. \quad (\text{A.31})$$

We pick up the discussion in the main part of the paper, at (5.36).

A.3. Field or H_0 branch

In the second system (A.9–A.10), the large-scale field H_0 is present but no large-scale flow. We write the system as $M\mathbf{v} = p\mathbf{v}$ with

$$M = \begin{pmatrix} -\eta k^2 & k & ik\tilde{B}_0(1+k^2)^{-1} \\ -\frac{1}{2}k & -\eta(1+k^2) & iB_0(1+k^2)^{-1} \\ \frac{1}{2}ik\tilde{B}_0(-1+k^2) & iB_0(1+k^2) & -\nu(1+k^2) \end{pmatrix}, \quad \mathbf{v} = \begin{pmatrix} H_0 \\ H_- \\ G_+ \end{pmatrix}. \quad (\text{A.32})$$

The matrix series for M now has

$$M_0 = \begin{pmatrix} 0 & 0 & 0 \\ 0 & -\eta & iB_0 \\ 0 & iB_0 & -\nu \end{pmatrix}, \quad M_1 = \begin{pmatrix} 0 & 1 & i\tilde{B}_0 \\ -\frac{1}{2} & 0 & 0 \\ -\frac{1}{2}i\tilde{B}_0 & 0 & 0 \end{pmatrix}, \quad M_2 = \begin{pmatrix} -\eta & 0 & 0 \\ 0 & -\eta & -iB_0 \\ 0 & iB_0 & -\nu \end{pmatrix}. \quad (\text{A.33})$$

We have that the inverse of the 2×2 block of M_0 is given as in (A.26) with ν and η interchanged and the same Δ . The calculation proceeds as before. At leading order in the eigenvalue problem (A.14) we take the same solution as that given in (A.27). At first order, we have

$$M_1 \mathbf{v}_0 = (0, -\frac{1}{2}, -\frac{1}{2}i\tilde{B}_0)^T. \quad (\text{A.34})$$

This gives $p_1 = 0$ and we solve (A.16) for \mathbf{v}_1 as

$$\mathbf{v}_1 = \frac{1}{2}\Delta(0, -\nu + \tilde{B}_0 B_0, -2iB_0)^T. \quad (\text{A.35})$$

At the next order (A.21) yields p_2 and so

$$p = p_2 k^2 + \dots = [\frac{1}{2}\Delta(-\nu + 3B_0^2/\eta) - \eta] k^2 + \dots, \quad (\text{A.36})$$

or, with $P = \nu/\eta$,

$$p = \left(\frac{P}{2\nu} \frac{-\nu^2 + 3B_0^2 P}{\nu^2 + B_0^2 P} - \frac{\nu}{P} \right) k^2 + \dots. \quad (\text{A.37})$$

Further analysis commences from equation (5.40).

Appendix B: Vertical strong field, with $U_0 = 0$, $\ell = 0$

In this appendix we turn to the vertical field system. Here there are two types of instability and two analyses that we will set out in this appendix and the next one. The calculation in this appendix is designed to capture the properties of the strong field branch seen for $\eta > \nu$ in figure 5 and is equivalent to that set out in Fraser *et al.* (2022). Mathematically we need to consider the limit when $B_0 \rightarrow \infty$ as $k \rightarrow 0$, and we find that relating these via $B_0 = O(k^{-1})$ is most informative. We will set the Bloch wavenumber $\ell = 0$ and take no mean flow $U_0 = 0$.

If we write out the vertical field equations truncated to G_0 , H_0 , $G_{\pm 1}$ and $H_{\pm 1}$, rewrite in terms of G_{\pm} and H_{\pm} defined in (A.5), then we obtain the equations (without any further approximation) in the form $M\mathbf{v} = p\mathbf{v}$ with

$$M = \left(\begin{array}{cc|cc} -\nu k^2 & ikB_0 & k(1+k^2)^{-1} & 0 \\ ikB_0 & -\eta k^2 & 0 & k \\ \hline \frac{1}{2}k(1-k^2) & 0 & -\nu(1+k^2) & ikB_0(1+k^2) \\ 0 & -\frac{1}{2}k & ikB_0(1+k^2)^{-1} & -\eta(1+k^2) \end{array} \right), \quad \mathbf{v} = \begin{pmatrix} G'_0 \\ H_0 \\ G_- \\ H_- \end{pmatrix}, \quad (\text{B.1})$$

where $G_0 = k^2 G'_0$ as usual. The fields G_+ and H_+ are decoupled (as we have $U_0 = 0$) and so not considered further. Before expanding M in powers of k , for strong vertical field we rescale $B_0 = k^{-1} B'_0$ with B'_0 fixed in the limit $k \rightarrow 0$. Then expanding M gives the matrices

$$M_0 = \left(\begin{array}{cc|cc} 0 & iB'_0 & 0 & 0 \\ iB'_0 & 0 & 0 & 0 \\ \hline 0 & 0 & -\nu & iB'_0 \\ 0 & 0 & iB'_0 & -\eta \end{array} \right), \quad M_1 = \left(\begin{array}{cc|cc} 0 & 0 & 1 & 0 \\ 0 & 0 & 0 & 1 \\ \hline \frac{1}{2} & 0 & 0 & 0 \\ 0 & -\frac{1}{2} & 0 & 0 \end{array} \right), \quad M_2 = \left(\begin{array}{cc|cc} -\nu & 0 & 0 & 0 \\ 0 & -\eta & 0 & 0 \\ \hline 0 & 0 & -\nu & iB'_0 \\ 0 & 0 & -iB'_0 & -\eta \end{array} \right). \quad (\text{B.2})$$

For an approximate growth rate p we use the expansion (A.14) and solve order by order. At leading order (A.15) we focus on the eigenvalues $p_0 = \pm iB'_0$ of M_0 , corresponding to large-scale undamped Alfvén waves. We will focus on the upper sign without loss of generality, and take

$$p_0 = iB'_0, \quad \mathbf{v}_0 = (1, 1, 0, 0)^T, \quad \mathbf{w}_0 = (1, 1, 0, 0). \quad (\text{B.3})$$

Here \mathbf{w}_0 is the left eigenvector as usual, with $\mathbf{w}_0(M_0 - p_0) = 0$ and $\mathbf{w}_0 \mathbf{v}_0 = 2$.

Moving to the first order, from (A.20) we rapidly find

$$M_1 \mathbf{v}_0 = (0, 0, \frac{1}{2}, -\frac{1}{2})^T, \quad p_1 = 0. \quad (\text{B.4})$$

We now need to solve (A.16) for \mathbf{v}_1 . To find a solution we clearly need only invert the 2×2 lower right block of $M_0 - p_0$ to calculate

$$\begin{pmatrix} -\nu - iB'_0 & iB'_0 \\ iB'_0 & -\eta - iB'_0 \end{pmatrix}^{-1} \begin{pmatrix} -\frac{1}{2} \\ \frac{1}{2} \end{pmatrix} = \frac{1}{2} \Delta \begin{pmatrix} \eta \\ -\nu \end{pmatrix} \quad (\text{B.5})$$

with the inverse determinant Δ now defined as

$$\Delta^{-1} = \eta\nu + iB'_0(\eta + \nu). \quad (\text{B.6})$$

Thus

$$\mathbf{v}_1 = \frac{1}{2} \Delta (0, 0, \eta, -\nu)^T. \quad (\text{B.7})$$

With this it is straightforward to calculate p_2 from (A.21)

$$p_2 = \frac{1}{4} \Delta (\eta - \nu) - \frac{1}{2} (\nu + \eta). \quad (\text{B.8})$$

Taking the real part of p_2 , and then putting back $B'_0 = kB_0$ and $p = p_0 + kp_1 + k^2 p_2 + \dots$, gives growth rates

$$\text{Re } p = \frac{\frac{1}{4} \nu \eta (\eta - \nu) k^2}{\nu^2 \eta^2 + k^2 B_0^2 (\nu + \eta)^2} - \frac{1}{2} (\nu + \eta) k^2 + \dots. \quad (\text{B.9})$$

This is taken up in the main body of the paper as (3.27).

Appendix C: Vertical weak field, with $U_0 \neq 0$, $\ell = 0$

We now continue with our analysis of vertical field instabilities for $\ell = 0$ and $U_0 \neq 0$. We studied the strong field branch with $B_0 = O(k^{-1})$ in the previous appendix. In the present appendix we will take $B_0 = O(k^2)$: this addresses the branch of vertical field instability as

seen in figure 4 and allows us to resolve the question of how magnetic field suppresses the purely hydrodynamic instability onset and reduces the critical value of ν below $\nu_c = 2^{-1/2}$. We will see that our results will be correct qualitatively even when B_0 is as large as order unity while $k \rightarrow 0$. Nonetheless it is convenient to refer to this as the ‘weak field branch’ to contrast with the strong field branch in the previous appendix.

We start with the matrix system (B.1) for instability in the presence of vertical field: $M\mathbf{v} = p\mathbf{v}$. However before expanding M_0 in powers of k we first rescale $B_0 = k^2 B'_0$, and set $\nu = \nu_0 + k^2 \nu_2 + \dots$, $\eta = \eta_0 + k^2 \eta_2 + \dots$. Here we are going to develop perturbation theory around the critical point $\nu_c(U_0)$ for the purely hydrodynamic problem, with $\nu_c(0) = 2^{-1/2}$. Expanding in powers of k yields

$$M_0 = \left(\begin{array}{ccc|ccc} 0 & 0 & 0 & 0 & 0 & 0 \\ 0 & -\nu_0 & -iU_0 & 0 & 0 & 0 \\ 0 & -iU_0 & -\nu_0 & 0 & 0 & 0 \\ \hline 0 & 0 & 0 & 0 & 0 & 0 \\ 0 & 0 & 0 & 0 & -\eta_0 & -iU_0 \\ 0 & 0 & 0 & 0 & -iU_0 & -\eta_0 \end{array} \right), \quad M_1 = \left(\begin{array}{ccc|ccc} 0 & 1 & 0 & 0 & 0 & 0 \\ \frac{1}{2} & 0 & 0 & 0 & 0 & 0 \\ 0 & 0 & 0 & 0 & 0 & 0 \\ \hline 0 & 0 & 0 & 0 & 1 & 0 \\ 0 & 0 & 0 & -\frac{1}{2} & 0 & 0 \\ 0 & 0 & 0 & 0 & 0 & 0 \end{array} \right), \quad (C.1)$$

$$M_2 = \left(\begin{array}{ccc|ccc} -\nu_0 & 0 & 0 & 0 & 0 & 0 \\ 0 & -\nu_0 - \nu_2 & 0 & 0 & 0 & 0 \\ 0 & 0 & -\nu_0 - \nu_2 & 0 & 0 & 0 \\ \hline 0 & 0 & 0 & -\eta_0 & 0 & 0 \\ 0 & 0 & 0 & 0 & -\eta_0 - \eta_2 & 0 \\ 0 & 0 & 0 & 0 & 0 & -\eta_0 - \eta_2 \end{array} \right), \quad M_3 = \left(\begin{array}{ccc|ccc} 0 & -1 & 0 & iB'_0 & 0 & 0 \\ -\frac{1}{2} & 0 & 0 & 0 & iB'_0 & 0 \\ 0 & 0 & 0 & 0 & 0 & iB'_0 \\ \hline iB'_0 & 0 & 0 & 0 & 0 & 0 \\ 0 & iB'_0 & 0 & 0 & 0 & 0 \\ 0 & 0 & iB'_0 & 0 & 0 & 0 \end{array} \right), \quad (C.2)$$

$$M_4 = \left(\begin{array}{ccc|ccc} -\nu_2 & 0 & 0 & 0 & 0 & 0 \\ 0 & -\nu_2 - \nu_4 & 0 & 0 & 0 & 0 \\ 0 & 0 & -\nu_2 - \nu_4 & 0 & 0 & 0 \\ \hline 0 & 0 & 0 & -\eta_2 & 0 & 0 \\ 0 & 0 & 0 & 0 & -\eta_2 - \eta_4 & 0 \\ 0 & 0 & 0 & 0 & 0 & -\eta_2 - \eta_4 \end{array} \right). \quad (C.3)$$

It will be convenient to let

$$\Delta^{-1} = \nu_0^2 + U_0^2, \quad \delta^{-1} = \eta_0^2 + U_0^2. \quad (C.4)$$

In keeping with the hydrodynamic case we will be expanding the system about a zero eigenvalue $p_0 = 0$ of M_0 with a flow field specified in G_0 . However we should note that p_0 is a twice repeated eigenvalue and we have two left and two right eigenvectors which we distinguish with \dagger and \ddagger :

$$\mathbf{v}_{0\dagger}^T = \mathbf{w}_{0\dagger} = (1, 0, 0, 0, 0, 0), \quad \mathbf{v}_{0\ddagger}^T = \mathbf{w}_{0\ddagger} = (0, 0, 0, 1, 0, 0). \quad (C.5)$$

In the perturbation theory for a general matrix M we would need to take \mathbf{v}_0 as a general combination of $\mathbf{v}_{0\dagger}$ and $\mathbf{v}_{0\ddagger}$, to be determined further in the expansion. However here, to avoid unnecessary algebra we will jump to the solution we need, and take

$$p_0 = 0, \quad \mathbf{v}_0 \equiv \mathbf{v}_{0\dagger}, \quad (C.6)$$

for a flow-dominated eigenfunction. We verify that this works as we delve into the expansion.

Looking to the first order equation (A.16) we apply $\mathbf{w}_{0\dagger}$ and $\mathbf{w}_{0\ddagger}$ to the left-hand side,

which only gives $p_1 = 0$ and we have

$$p_1 = 0, \quad M_0 \mathbf{v}_1 = (0, -\frac{1}{2}, 0, 0, 0, 0)^T. \quad (\text{C.7})$$

However when we solve for \mathbf{v}_1 we can add not only a multiple of \mathbf{v}_0 to the solution (which would have no effect in the calculation) but also a multiple of the purely magnetic eigenvector $\mathbf{v}_{0\ddagger}$. Thus we solve for \mathbf{v}_1 in the form

$$\mathbf{v}_1 = (0, \frac{1}{2}\nu_0\Delta, -\frac{1}{2}iU_0\Delta, b, 0, 0)^T, \quad (\text{C.8})$$

where b is an unknown constant, to be determined.

At the next order we will aim to take $p_2 = 0$ so as to push various the effects down the series in powers of k : this is achieved if we fix $\Delta = 2$. Thus at second order we set

$$p_2 = 0, \quad \Delta = 2, \quad (\text{C.9})$$

and note that this then fixes

$$\nu_0 \equiv \nu_c(U_0) = (\frac{1}{2} - U_0^2)^{1/2}. \quad (\text{C.10})$$

This is the critical value for onset for the pure hydrodynamic case, with a mean flow but with zero magnetic field. A strong enough mean flow $|U_0| > 2^{-1/2}$ is enough to suppress any instability and so from now on we take $U_0^2 < \frac{1}{2}$ so that ν_0 is real and positive.

We then need to solve (A.17) which amounts to

$$M_0 \mathbf{v}_2 = (0, 0, 0, 0, \frac{1}{2}b, 0)^T, \quad (\text{C.11})$$

a suitable solution being

$$\mathbf{v}_2 = (0, 0, 0, 0, -\frac{1}{2}\eta_0 b \delta, \frac{1}{2}iU_0 b \delta)^T. \quad (\text{C.12})$$

It turns out that we do not gain any further information in the ensuing calculation if we incorporate an unknown multiple of $\mathbf{v}_{0\ddagger}$ in our solution for \mathbf{v}_2 , at this order, and so we do not.

At third order, applying $\mathbf{w}_{0\ddagger}$ and $\mathbf{w}_{0\ddagger}$ to (A.18) gives

$$p_3 = 0, \quad b = \eta_0^{-1}(1 + \frac{1}{2}\delta)^{-1}iB'_0, \quad (\text{C.13})$$

and we then solve

$$M_0 \mathbf{v}_3 = (0, \frac{1}{2} + \frac{1}{2}(\nu_0 + \nu_2)\nu_0\Delta, -\frac{1}{2}(\nu_0 + \nu_2)iU_0\Delta, 0, 0, 0)^T, \quad (\text{C.14})$$

for \mathbf{v}_3 with

$$\mathbf{v}_3 = (0, -\frac{1}{2}\nu_0\Delta - \frac{1}{2}(\nu_0 + \nu_2)(\nu_0^2 - U_0^2)\Delta^2, \frac{1}{2}iU_0\Delta + (\nu_0 + \nu_2)iU_0\nu_0\Delta^2, 0, 0, 0)^T, \quad (\text{C.15})$$

Finally applying $\mathbf{w}_{0\ddagger}$ and $\mathbf{w}_{0\ddagger}$ to (A.19) gives our desired growth rate

$$p_4 = -\nu_2 - \nu_0\Delta + iB'_0 b - \frac{1}{2}(\nu_0 + \nu_2)(\nu_0^2 - U_0^2)\Delta^2 \quad (\text{C.16})$$

We now put $p = p_4 k^4 + \dots$, and substitute b from (C.13), $\Delta = 2$, $B'_0 = k^{-2}B_0$, $\eta_0 = \nu_0/P$, also replacing U_0 in terms of $\nu_0 = \nu_c$ and $\nu_2 = k^{-2}(\nu - \nu_c) + \dots$, to find

$$p = -\frac{P}{\nu_c(1 + \frac{1}{2}\delta)} B_0^2 + 4\nu_c^2(\nu_c - \nu)k^2 - \nu_c(1 + 4\nu_c^2)k^4 + \dots, \quad (\text{C.17})$$

with

$$\nu_c = \sqrt{\frac{1}{2} - U_0^2}, \quad \delta = \frac{P^2}{\nu_c^2(1 - P^2) + \frac{1}{2}P^2}. \quad (\text{C.18})$$

This is the general formula for the growth rate $p(k, \nu, B_0, P, U_0)$ including a mean flow U_0 with $U_0^2 < \frac{1}{2}$ (so that ν_c is defined as a positive number).

In the case of zero mean flow, $U_0 = 0$, we have $\nu_c = 2^{-1/2}$, $\delta = 2P^2$, and this simplifies to

$$p = -\frac{\sqrt{2}P}{1+P^2} B_0^2 + 2\left(\frac{1}{\sqrt{2}} - \nu\right)k^2 - \frac{3}{\sqrt{2}}k^4 + \dots \quad (\text{C.19})$$

We continue the discussion in the main body of the paper; see equations (3.24, 3.25). Note that going to fourth order here suggests that the modes $G_{\pm 2}$ and $H_{\pm 2}$ might also be needed to give a correct evaluation of p_4 ; this needed to be checked and was — we found that the couplings are too weak, in terms of the powers of k involved, to give a contribution to the growth rate to the order taken above.

Appendix D: Horizontal field, with $U_0 = 0$, $\ell \neq 0$

Our final calculation brings in the Bloch wavenumber ℓ . This can be done in the case of vertical field (Algaatheem 2023), but there increasing ℓ from zero seems to have only the effect of suppressing the $\ell = 0$ instability, so we do not consider this further. We instead study horizontal field, where having $\ell \neq 0$ can enhance instability. We take $U_0 = 0$ to keep the problem manageable. We omit straightforward but messy details and in fact will only go up to first order in perturbation theory.

Our starting point is the equations (4.34, 4.35) with n replaced by $n + \ell$, and we consider only the modes $G_0, G_{\pm 1}, H_0, H_{\pm 1}$. We set, as in the original horizontal field problem (appendix A),

$$G_0 = k^2 G'_0, \quad \tilde{B}_0 = B_0/\eta. \quad (\text{D.1})$$

Once we have $\ell \neq 0$ in the problem, we have to ask how ℓ scales as $k \rightarrow 0$. It turns out that the appropriate scaling to gain useful results is

$$\ell = k\ell' = O(k), \quad (\text{D.2})$$

so we hold ℓ' and G'_0 constant while $k \rightarrow 0$. We now follow the usual procedure of making these substitutions, expressing the equations in terms of $G_0, G_{\pm}, H_0, H_{\pm}$ and writing the system as $M\mathbf{v} = p\mathbf{v}$ with

$$\mathbf{v} = \begin{pmatrix} G'_0 \\ G_- \\ H_+ \\ H_0 \\ H_- \\ G_+ \end{pmatrix}, \quad (\text{D.3})$$

and $M = M_0 + kM_1 + \dots$ with

$$M_0 = \left(\begin{array}{ccc|ccc} 0 & 0 & 0 & 0 & 2\ell' i\tilde{B}_0 & 2\ell' \\ 0 & -\nu & iB_0 & 0 & 0 & 0 \\ 0 & iB_0 & -\eta & 0 & 0 & 0 \\ \hline 0 & 0 & 0 & 0 & 0 & 0 \\ 0 & 0 & 0 & 0 & -\eta & iB_0 \\ 0 & 0 & 0 & 0 & iB_0 & -\nu \end{array} \right), \quad (\text{D.4})$$

and

$$\mathbf{M}_1 = \left(\begin{array}{ccc|ccc} 0 & 1 - 3\ell'^2 & i\tilde{B}_0(1 + \ell'^2) & iB_0\ell'(1 + \ell'^2) & 0 & 0 \\ \frac{1}{2}(1 + \ell'^2)^{-1} & 0 & 0 & 0 & iB_03\ell' & -2\ell'\nu \\ \frac{1}{2}i\tilde{B}_0(1 + \ell'^2)^{-1} & 0 & 0 & 0 & -2\ell'\eta & -iB_0\ell' \\ \hline iB_0\ell'(1 + \ell'^2)^{-1} & 0 & 0 & 0 & 1 & i\tilde{B}_0 \\ 0 & -iB_0\ell' & -2\ell'\eta & -\frac{1}{2} & 0 & 0 \\ 0 & -2\ell'\nu & iB_03\ell' & -\frac{1}{2}i\tilde{B}_0 & 0 & 0 \end{array} \right). \quad (\text{D.5})$$

It is convenient to set

$$\Delta^{-1} = \nu\eta + B_0^2. \quad (\text{D.6})$$

We are now ready to calculate p . The matrix M_0 has now lost the attractive block structure present in the earlier expansions as a consequence of the scaling of ℓ . Nonetheless M_0 has a double zero eigenvalue $p_0 = 0$ with right eigenvectors

$$\mathbf{v}_{0\uparrow} = (1, 0, 0, 0, 0, 0)^T, \quad \mathbf{v}_{0\downarrow} = (0, 0, 0, 1, 0, 0)^T, \quad (\text{D.7})$$

and left eigenvectors

$$\mathbf{w}_{0\uparrow} = (1, 0, 0, 0, 2\ell'\Delta\eta^{-1}iB_0(\nu + \eta), 2\ell'\Delta\eta^{-1}(\eta^2 - B_0^2)), \quad \mathbf{w}_{0\downarrow} = (0, 0, 0, 1, 0, 0). \quad (\text{D.8})$$

In the previous case of a double-zero eigenvalue (in appendix C) we anticipated the structure of \mathbf{v}_0 (as dominated by the hydrodynamic field G_0). Here we cannot do so and so we set

$$\mathbf{v}_0 = b\mathbf{v}_{0\uparrow} + c\mathbf{v}_{0\downarrow}, \quad (\text{D.9})$$

for some constants b and c .

Now, looking at the first order equation (A.16), namely $p_1\mathbf{v}_0 = (M_0 - p_0)\mathbf{v}_1 + M_1\mathbf{v}_0$ with $p_0 = 0$, we can apply either of the two vectors $\mathbf{w}_{0\uparrow}$ and $\mathbf{w}_{0\downarrow}$ on the left, to gain two equations,

$$p_1b = \mathbf{w}_{0\uparrow}M_1\mathbf{v}_0 = iB_0\ell'[1 + \ell'^2 + \Delta\eta^{-2}(B_0^2 - \nu\eta - 2\eta^2)]c, \quad (\text{D.10})$$

$$p_1c = \mathbf{w}_{0\downarrow}M_1\mathbf{v}_0 = iB_0\ell'(1 + \ell'^2)^{-1}b. \quad (\text{D.11})$$

Together, these yield

$$p_1^2 = -B_0^2\ell'^2[1 + (1 + \ell'^2)^{-1}\Delta\eta^{-2}(B_0^2 - \nu\eta - 2\eta^2)], \quad (\text{D.12})$$

and so, putting back $\ell' = \ell/k$ and Δ we find the growth rate as

$$p = \pm B_0\ell \left[\frac{k^2}{\ell^2 + k^2} \frac{\nu\eta + 2\eta^2 - B_0^2}{\eta^2(\nu\eta + B_0^2)} - 1 \right]^{1/2} + \dots \quad (\text{D.13})$$

We have gained this equation by only going to the first order matrix M_1 , but it reveals an instability that crucially relies on having a non-zero Bloch wavenumber, $\ell \neq 0$. We continue our discussion in the main body of the paper, from (5.44).

Acknowledgements

ADG acknowledges support from the EPSRC Research Grant EP/T023139/1 and AH acknowledges support from the STFC Research Grant ST/V000659/1. AMA is grateful for a

PhD studentship awarded by the government of Saudi Arabia. For the purpose of open access, the author has applied a Creative Commons Attribution (CC BY) licence to any Author Accepted Manuscript version arising.

Data access statement

No data were created or analysed in this study.

References

- Algaatheem, A.M., Jets and instabilities in forced MHD flows, in preparation. Ph.D. Thesis, University of Exeter Unpublished thesis, 2023.
- Balmforth, N.J. and Young, Y.N., Stratified Kolmogorov flow. *Journal of Fluid Mechanics*, 2002, **450**, 131–167.
- Boffetta, G., Celani, A. and Prandi, R., Large scale instabilities in two-dimensional magnetohydrodynamics. *Physical Review E*, 2000, **61**, 4329.
- Bouchet, F., Nardini, C. and Tangarife, T., Kinetic theory of jet dynamics in the stochastic barotropic and 2D Navier-Stokes equations. *Journal of Statistical Physics*, 2013, **153**, 572–625.
- Chechkin, A., Negative magnetic viscosity in two dimensions. *Journal of Experimental and Theoretical Physics*, 1999, **89**, 677–688.
- Constantinou, N.C. and Parker, J.B., Magnetic suppression of zonal flows on a beta plane. *The Astrophysical Journal*, 2018, **863**, 46.
- Dubrulle, B. and Frisch, U., Eddy viscosity of parity-invariant flow. *Physical Review A*, 1991, **43**, 5355.
- Durstun, S. and Gilbert, A.D., Transport and instability in driven two-dimensional magnetohydrodynamic flows. *Journal of Fluid Mechanics*, 2016, **799**, 541–578.
- Farrell, B.F. and Ioannou, P.J., Formation of jets by baroclinic turbulence. *Journal of the Atmospheric Sciences*, 2008, **65**, 3353–3375.
- Fraser, A., Cresswell, I. and Garaud, P., Non-ideal instabilities in sinusoidal shear flows with a streamwise magnetic field. *Journal of Fluid Mechanics*, 2022, **949**, A43.
- Frisch, U., Legras, B. and Villone, B., Large-scale Kolmogorov flow on the beta-plane and resonant wave interactions. *Physica D: Nonlinear Phenomena*, 1996, **94**, 36–56.
- Galperin, B., Sukoriansky, S., Dikovskaya, N., Read, P., Yamazaki, Y. and Wordsworth, R., Anisotropic turbulence and zonal jets in rotating flows with a β -effect. *Nonlinear Processes in Geophysics*, 2006, **13**, 83–98.
- Hughes, D.W., Rosner, R. and Weiss, N.O., *The solar tachocline*, 2007 (Cambridge University Press).
- Kim, E.j., Role of magnetic shear in flow shear suppression. *Physics of Plasmas*, 2007, **14**, 084504.
- Leprovost, N. and Kim, E.j., Turbulent transport and dynamo in sheared magnetohydrodynamics turbulence with a nonuniform magnetic field. *Physical Review E*, 2009, **80**, 026302.
- Lucas, D. and Kerswell, R., Spatiotemporal dynamics in two-dimensional Kolmogorov flow over large domains. *Journal of Fluid Mechanics*, 2014, **750**, 518–554.
- Lucas, D. and Kerswell, R.R., Recurrent flow analysis in spatiotemporally chaotic 2-dimensional Kolmogorov flow. *Physics of Fluids*, 2015, **27**, 045106.
- Manfroi, A. and Young, W., Stability of β -plane Kolmogorov flow. *Physica D: Nonlinear Phenomena*, 2002, **162**, 208–232.
- Meshalkin, L. and Sinai, I.G., Investigation of the stability of a stationary solution of a system of equations for the plane movement of an incompressible viscous liquid. *Journal of Applied Mathematics and Mechanics*, 1961, **25**, 1700–1705.
- Nepomniashchii, A., On stability of secondary flows of a viscous fluid in unbounded space: PMM vol. 40, no. 5, 1976, pp. 886–891. *Journal of Applied Mathematics and Mechanics*, 1976, **40**, 836–841.
- Parker, J.B. and Constantinou, N.C., Magnetic eddy viscosity of mean shear flows in two-dimensional magnetohydrodynamics. *Physical Review Fluids*, 2019, **4**, 083701.
- Parker, J.B. and Krommes, J.A., Generation of zonal flows through symmetry breaking of statistical homogeneity. *New Journal of Physics*, 2014, **16**, 035006.
- Read, P.L., Yamazaki, Y.H., Lewis, S.R., Williams, P.D., Wordsworth, R., Miki-Yamazaki, K., Sommeria, J. and Didelle, H., Dynamics of convectively driven banded jets in the laboratory. *Journal of the Atmospheric Sciences*, 2007, **64**, 4031–4052.
- Scott, R.K. and Dritschel, D.G., The structure of zonal jets in geostrophic turbulence. *Journal of Fluid Mechanics*, 2012, **711**, 576–598.
- She, Z.S., Metastability and vortex pairing in the Kolmogorov flow. *Physics Letters A*, 1987, **124**, 161–164.

REFERENCES

29

- Sivashinsky, G.I., Weak turbulence in periodic flows. *Physica D: Nonlinear Phenomena*, 1985, **17**, 243–255.
- Srinivasan, K. and Young, W., Zonostrophic instability. *Journal of the Atmospheric Sciences*, 2012, **69**, 1633–1656.
- Tobias, S., Dagon, K. and Marston, J., Astrophysical fluid dynamics via direct statistical simulation. *The Astrophysical Journal*, 2011, **727**, 127.
- Tobias, S.M., Diamond, P.H. and Hughes, D.W., β -plane magnetohydrodynamic turbulence in the solar tachocline. *The Astrophysical Journal*, 2007, **667**, L113.
- Vallis, G.K. and Maltrud, M.E., Generation of mean flows and jets on a beta plane and over topography. *Journal of Physical Oceanography*, 1993, **23**, 1346–1362.